

# Stellar-mass black holes in young massive and open stellar clusters and their role in gravitational-wave generation II

Sambaran Banerjee<sup>1,2★</sup>

<sup>1</sup>*Argelander-Institut für Astronomie (AlfA), Auf dem Hügel 71, D-53121, Bonn, Germany*

<sup>2</sup>*Helmholtz-Instituts für Strahlen- und Kernphysik (HISKP), Nussallee 14-16, D-53115 Bonn, Germany*

October 15, 2018

## ABSTRACT

The study of stellar-remnant black holes (BH) in dense stellar clusters is now in the spotlight, especially due to their intrinsic ability to form binary black holes (BBH) through dynamical encounters, that potentially coalesce via gravitational-wave (GW) radiation. In this work, which is a continuation from a recent study (Paper I), additional models of compact stellar clusters with initial masses  $\lesssim 10^5 M_\odot$  and also those with small fractions of primordial binaries ( $\lesssim 10\%$ ) are evolved for long term, applying the direct N-body approach, assuming state-of-the-art stellar-wind and remnant-formation prescriptions. That way, a substantially broader range of computed models than that in Paper I is achieved. As in Paper I, the general-relativistic BBH mergers continue to be mostly mediated by triples that are bound to the clusters rather than happen among the ejected BBHs. In fact, the number of such in situ BBH mergers, per cluster, tend to increase significantly with the introduction of a small population of primordial binaries. Despite the presence of massive primordial binaries, the merging BBHs, especially the in situ ones, are found to be exclusively dynamically assembled and hence would be spin-orbit misaligned. The BBHs typically traverse through both the LISA’s and the LIGO’s detection bands, being audible to both instruments. The “dynamical heating” of the BHs keeps the Electron-Capture-Supernova (ECS) neutron stars (NS) from effectively mass segregating and participating in exchange interactions; the dynamically-active BHs would also exchange into any NS binary within  $\lesssim 1$  Gyr. Such young massive and open clusters have the potential to contribute to the dynamical BBH merger detection rate to a similar extent as their more massive globular-cluster counterparts.

**Key words:** open clusters and associations: general – globular clusters: general – stars: kinematics and dynamics – stars: black holes – methods: numerical – gravitational waves

## 1 INTRODUCTION

The study of dynamical interactions of black holes (hereafter BH) in dense stellar systems is now nearly 30 years old and is still gaining momentum. A key point of interest in such a process is its inherent potential of generating gravitational waves (hereafter GW) from the general-relativistic (hereafter GR) inspiral of dynamically-formed binary black holes (hereafter BBH; Kulkarni et al. 1993; Sigurdsson & Hernquist 1993; Portegies Zwart & McMillan 2000). The interest in this line of study has naturally got rejuvenated after the landmark detections of GW, from BBH inspiral events, by the Advanced Laser Interferometer Gravitational-Wave Observatory (hereafter LIGO; Abbott et al. 2016c) detec-

tor, namely, GW150914 (Abbott et al. 2016c,e), GW151226 (Abbott et al. 2016d), and the “trigger” event LVT151012 (Abbott et al. 2016c). Especially, the most recent LIGO detection, namely, the BBH inspiral event GW170104 (Abbott et al. 2017) prefer a spin-orbit misalignment among the merging BHs (which may, moreover, be an anti-alignment; see also Abbott et al. 2016a,b; Farr et al. 2017), provided the BHs’ spins are large; the detection is, however, as well consistent with zero or small BH spins. A spin-orbit misaligned merger opens up the possibility that the members of the merging BH pair might have been born independently and paired up later, which is exactly what the dynamical scenarios achieve in an inherent way. Of course, spin-orbit misaligned BBH coalescences can, as well, be potentially obtained via evolution of isolated, massive-stellar binaries (see below).

★ E-mail: sambaran@astro.uni-bonn.de (SB)

In a nutshell, the dynamical formation of (stellar-mass) BBHs in star clusters is a rather straightforward process: if a certain number of BHs receive sufficiently low natal kicks, during their formation through core collapse of massive stars (*e.g.*, in the case of a direct collapse or “failed supernova”), that they remain bound to the gravitational potential of the cluster, they would segregate to the innermost regions of the cluster. Depending on the number of BHs retained in the cluster at birth and their masses (which is  $\sim 10$  to  $\sim 100$  times the cluster’s average stellar mass depending on their progenitor stars’ wind; see below), the collection of bound BHs might undergo a runaway mass segregation (mass-stratification or Spitzer instability; [Spitzer 1987](#)) to form a central and highly dense subsystem of BHs, where they would continuously interact. Otherwise, the dynamical friction due to the dense stellar environment of the cluster would as well act to keep the BHs centrally concentrated (as these BHs are much more massive than the normal stars, they would always segregate towards the cluster’s center simply via dynamical friction, rather than being driven by the two-body relaxation among the average stars). In either case, it should be borne in mind that as long as the BHs retain in the cluster, they continue to interact with the rest of the stellar entities and not only among themselves, *i.e.*, they do *not* comprise a so-called “dynamically isolated subsystem” ([Morscher et al. 2013](#); [Breen & Hoggie 2013a](#)). Such interactions happen, both, in the form of close encounters between the BHs (or the BBHs) and the individual stars or stellar binaries (*e.g.*, tidal capture, exchange) and of the overall interaction between the BHs with the stellar background (the dynamical friction).

Such a dense BH core serves as a factory for dynamically pairing BBHs, often via the three-body mechanism ([Spitzer 1987](#); [Hoggie & Hut 2003](#)). If primordial stellar binaries are present, they would as well mediate the pairing process (see, *e.g.*, [Rodríguez et al. 2016a](#); [Chatterjee et al. 2017a](#)). The subsequent frequent and super-elastic ([Spitzer 1987](#)) encounters of a BBH with other single BHs and BBHs serve as a recipe for (a) injecting kinetic energy (K.E.) into the BH sub-cluster and as well into the whole star cluster causing the latter to expand ([Mackey et al. 2007, 2008](#)), (b) ejecting single and binary BHs from the cluster depleting the BH population, and (c) forming triple-BH systems within the BH-core. The ejected BBHs are typically dynamically tightened (hardened; [Hoggie 1975](#)) and also eccentric, an adequate combination of which ([Peters 1964](#)) would lead to the inspiral via GW radiation and the coalescence of a BBH within the Hubble time.

The triple-BHs that are bound to the clusters, on the other hand, would typically undergo a large eccentricity boost and hence potentially GW inspiral and coalescence, of the inner binary. If the triple is hierarchical and sufficiently long lasting, this would be due to the classical/secular eccentric Kozai oscillations ([Kozai 1962](#); [Miller & Hamilton 2002](#); [Wen 2003](#); [Lithwick & Naoz 2011](#); [Antonini et al. 2014](#); [Hoang et al. 2017](#)). However, triples, that trigger eccentricity boost and hence GR coalescence, can as well be intermediate, metastable (or democratic) systems which disintegrate (if GR effects are excluded), typically, after a few internal orbits of the triple; see, *e.g.*, [Hut & Bahcall \(1983\)](#); [Samsing et al. \(2014\)](#). The latter type of triples can be either an intermediate phase of a resonant BBH-BH interaction or an

outcome of a close interaction between two BBHs of similar binding energies. Hierarchical, stable configurations, on the other hand, are more likely to arise during interactions between two BBHs where one is much tighter than the other. A sufficient eccentricity boost of the triple’s constituent BBH, either during a metastable, resonant interaction phase ([Samsing et al. 2014](#)) or due to a regular Kozai oscillation, would initiate its GR inspiral, provided this happens before the triple gets either disintegrated through its internal dynamical evolution or perturbed by an intruder. The eccentricity boost is instrumental here; the GR inspiral and merger of a sufficiently tight, (nearly) circular BBH is practically impossible while being bound to a stellar cluster since a BBH would get ejected due to dynamical interactions well before it achieves the required tightness (but this may be possible in galactic nuclei where the escape speed is typically  $> 100 \text{ km s}^{-1}$ ). In other words, although a star cluster continues to eject single and binary BHs and form BH triples until its BH reservoir is (nearly) depleted, the occurrence of a dynamical BBH inspiral is quite a coincidence but is inherent to the dense stellar environment.

Since 1990s, aspects of the above mechanism is studied at various levels of detail. Following preliminary but pioneering studies such as [Kulkarni et al. \(1993\)](#); [Sigurdsson & Hernquist \(1993\)](#); [Portegies Zwart & McMillan \(2000\)](#), more recent direct N-body (*e.g.*, [Banerjee et al. 2010](#); [Aarseth 2012](#); [Sippel & Hurley 2013](#); [Ziosi et al. 2014](#); [Kimpson et al. 2016](#); [Wang et al. 2016](#); [Hurley et al. 2016](#); [Mapelli 2016](#); [Baumgardt 2017](#); [Banerjee 2017](#); [Park et al. 2017](#)) and Monte-Carlo (*e.g.*, [Downing et al. 2010](#); [Downing et al. 2011](#); [Morscher et al. 2015](#); [Rodríguez et al. 2016a,c](#); [Chatterjee et al. 2017a,b](#); [Askar et al. 2016](#)) calculations of model stellar clusters study the dynamically-driven depletion of BHs, the resulting feedback onto the cluster and the dynamically-induced BBH inspirals self consistently and in much more detail. Adopting somewhat simpler but realistic conditions, detailed semi-analytic studies of these aspects have also been performed recently ([Breen & Hoggie 2013a,b](#); [Arca-Sedda 2016](#)). Also, such a semi-analytic modelling, in the context of  $\sim 10^7 M_\odot$  nuclear stellar clusters, has been recently conducted by [Antonini & Rasio \(2016\)](#) and the possibility of BBH coalescences resulting from triple stars in the field has been studied by [Silsbee & Tremaine \(2017\)](#); [Antonini et al. \(2017\)](#). By nature, Monte-Carlo calculations are restricted to massive model clusters, typically of  $\sim 10^5 M_\odot - 10^6 M_\odot$ , that are representatives (or progenitors) of classical globular clusters (hereafter GC). On the other hand, due to high computational cost, direct N-body calculations are typically done with clusters of  $\lesssim 10^5 M_\odot$ . However, in the “Dragon Simulations” ([Wang et al. 2016](#)), clusters that are relatively extended, with half-mass radii of  $\approx 3 - 8 \text{ pc}$ , but comprising as many as  $N \approx 10^6$  stars (they can also be taken as representatives of galactic nuclear clusters) are evolved, with the direct N-body program NBODY6++ ([Wang et al. 2015](#)), for nearly a Hubble time on large GPU compute clusters.

The typical conclusion from such studies is that the local dynamical BBH inspiral rate (density) is  $\approx 5 - 10 \text{ yr}^{-1} \text{ Gpc}^{-3}$ , that would contribute several 10s of BBH inspiral detection per year with the LIGO, given its proposed full sensitivity ([Banerjee et al. 2010](#); [Rodríguez et al. 2015](#); [Askar et al. 2016](#); [Banerjee 2017](#); [Park et al. 2017](#)). However, taking into account lower-mass, open-type clus-

ters, Banerjee (2017) anticipate a full-sensitivity dynamical BBH detection rate up to  $\sim 100$  per year. In the majority of these numerical studies (but see Banerjee 2017; below), most of the GW coalescences have occurred among BBHs that are dynamically ejected from the clusters. Another important corollary is that the BH population in massive clusters, although decaying monotonically with time due to the dynamical interactions and the resulting ejections, it never actually gets completely depleted even in a Hubble time, so that a substantial population of BHs would be retained even in old GCs. In contrast, in the earliest studies (*e.g.*, Kulkarni et al. 1993), it was conceived that all except one or two BHs would be ejected out of an old cluster, making them unpopular hosts of stellar-remnant BHs. Essentially, such a long-term retention is due to the energy generation through dynamical encounters in the BH-core (see above) that results in substantial expansion of both the parent cluster and the BH-core itself (see, *e.g.*, Fig. 6 & 7 of Banerjee 2017), suppressing the BH-BH interaction rate. This “self-regulation” causes the BH population to decline but exponentially; such a self-regulatory behaviour is essentially a manifestation of the Hénon (1975) principle, according to which the central (dynamical) energy generation of a (post-core-collapse) cluster is controlled by the energy demands of the bulk of the cluster. This principle is analogously applicable to the energy generation due to dynamical encounters within the BH-core inside a stellar cluster, as done in the semi-analytic study by Breen & Hoggie (2013a). This behaviour is consistent with the recent identification of stellar-mass BH candidates in Galactic GCs (see below).

Space-based X-ray observation has been the most popular approach to identify BH candidates in GCs, *e.g.*, Maccarone et al. (2007); Brassington et al. (2010); Lützgendorf et al. (2016). However, the best stellar-mass BH candidates have been identified only recently by comparing X-ray and radio fluxes from localized sources in the GCs M22 (Strader et al. 2012) and 47 Tuc (Miller-Jones et al. 2015). Given the rather small probability of formation of BH X-ray binaries, the presence of such candidates may indicate the existence of a much larger population of stellar-mass BHs in GCs (see Strader et al. 2012 and references therein). In fact, the recently-discovered very high mass-to-light-ratio GCs or “dark star clusters” (DSC; Banerjee & Kroupa 2011; Taylor et al. 2015; Bovill et al. 2016; Sollima et al. 2016) provide additional indications of the possible presence of large populations of dark remnants in GCs.

Alternatively, BBHs can be formed through the evolution of isolated massive-stellar binaries in the field. Such scenarios stem on either common-envelope (CE) evolution (Belczynski et al. 2016) or chemically-homogeneous evolution (De Mink et al. 2009; De Mink & Mandel 2016; Marchant et al. 2016) of massive binaries. In fact, GW170104 event is still consistent with no or small BH spins (*i.e.*, with non-detection of BH spins), in which case it can be reproduced through isolated massive-binary evolution also (but preferably with modified physics; see Belczynski et al. 2017); a spin-orbit misalignment (but preferably positive) can also be reproduced from such a channel (Belczynski et al. 2016, 2017; O’Shaughnessy et al. 2017a). In such studies, BBH inspiral detection rate of  $\sim 10 - \sim 1000 \text{ yr}^{-1}$  has been estimated for the LIGO (at its proposed full sensitivity; *i.e.*, up to 2 orders of magnitudes higher detection rate than what is

estimated for dynamically-formed BBHs). Tight BBH formation through massive-binary evolution in isolation, and hence their merger rate, depends on the nature of CE evolution, tidal interactions among massive stars, and their structural details, all of which are still poorly understood. In that sense, the dynamical mechanism is, so far, the most assured channel for BBH formation and their mergers.

Recently, Banerjee (2017, hereafter Paper I) has computed a preliminary set of evolutionary models of stellar clusters with initial masses  $1.0 \times 10^4 M_\odot - 5.0 \times 10^4 M_\odot$ , half-mass radii 1-2 pc, that is typical for young massive clusters (hereafter YMC) and starburst clusters, and having metallicities between  $0.05 Z_\odot - Z_\odot$ . Including the state-of-the-art stellar-wind and remnant-formation schemes of Belczynski et al. (2010b), that allows the formation of direct-collapse (or failed-supernova) black holes (hereafter DCBH; Belczynski et al. 2008; Spera et al. 2015), these models were evolved, all the way from their young age until their dissolution or at least 10 Gyr age, for the first time with the direct N-body technique (utilizing NBODY7, a descendant of NBODY6; see Sec. 2.1), where all sorts of dynamical encounters are treated completely and self-consistently. These comprise the most advanced simulations of the dynamics of BHs in a star cluster to date. The motivation for the study was that with decreasing metallicity, not only the average BH mass increases but also their mass spectrum widens (Belczynski et al. 2010b) — an effect that is particularly pronounced for the adopted stellar-wind and remnant-formation recipes that comfortably include all the LIGO-detected BHs (Abbott et al. 2016e). This would, in turn, modify the nature of the dynamical interactions among the BHs and hence the BBH production.

An interesting fact, that became apparent from the computations in Paper I is that, in general and irrespective of the cluster’s metallicity, the number of (triple-induced; see above) BBH mergers happening while being bound to the model cluster well exceeds that happening among the ejected BBHs (see Table 1 of Paper I). This is in contrast to what Monte-Carlo calculations of similarly and more massive systems but with similar model ingredients (*e.g.*, Morscher et al. 2015; Rodriguez et al. 2016a; Chatterjee et al. 2017a; Askar et al. 2016), have found and also to the outcomes of direct N-body calculations with equal- or binary-mass BHs (*e.g.*, Banerjee et al. 2010; Park et al. 2017). As discussed in the Sec. 3.2 of Paper I, this difference could be partly due to the way in which compact subsystems are treated in Monte Carlo-based models and partly due to the broad BH mass functions adopted in Paper I, that has not been properly explored through the direct N-body method until Paper I (but see Park et al. 2017).

The present work is a continuation of the study started in Paper I, where additional model computations are performed, resulting in a broader mass spectrum of the model star clusters. Furthermore, a preliminary set of models, that include a primordial-binary population, is computed. Due to a broader BH mass spectrum, and hence the potential for more interesting dynamics among the BHs, only lower metallicities, of  $Z \leq 0.50 Z_\odot$ , are considered for the newer models. This naturally places the majority of the models in dwarf galaxy-like hosts (see also O’Shaughnessy et al. 2017b in this context); the most massive ones can as well be looked upon as progenitors of present-day GCs which, on an aver-

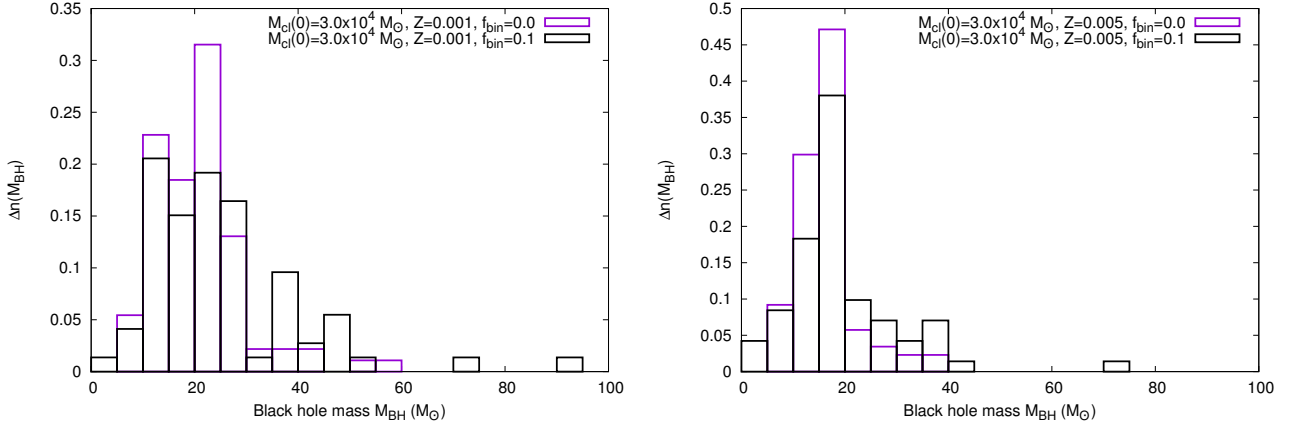


**Figure 1.** The (normalized) mass distributions of the BHs formed in the  $M_{cl}(0) \approx 3.0 \times 10^4 M_{\odot}$  models with initially only single stars (blue-lined boxes) and with  $f_{bin} \approx 10\%$  overall primordial binaries (black-lined boxes), for  $Z = 0.05Z_{\odot}$  (left) and  $0.25Z_{\odot}$  (right). The modified BH mass distributions in the primordial-binary cases are the combined outcomes of the internal evolution and dynamical modifications of the massive primordial binaries. Given that the BH-progenitor stars, in the models with primordial binaries, have nearly  $f_{obin} \approx 100\%$  primordial binary fraction (as opposed to the much lower overall binary fraction; see Sec. 2), all the BHs in such models are either born in a binary or/and have their masses affected by (dynamically-modified) binary evolution. The typical resultant is a wider BH mass distribution, due to the massive binaries’ mergers, CE phases, and tidally-enhanced stellar winds.

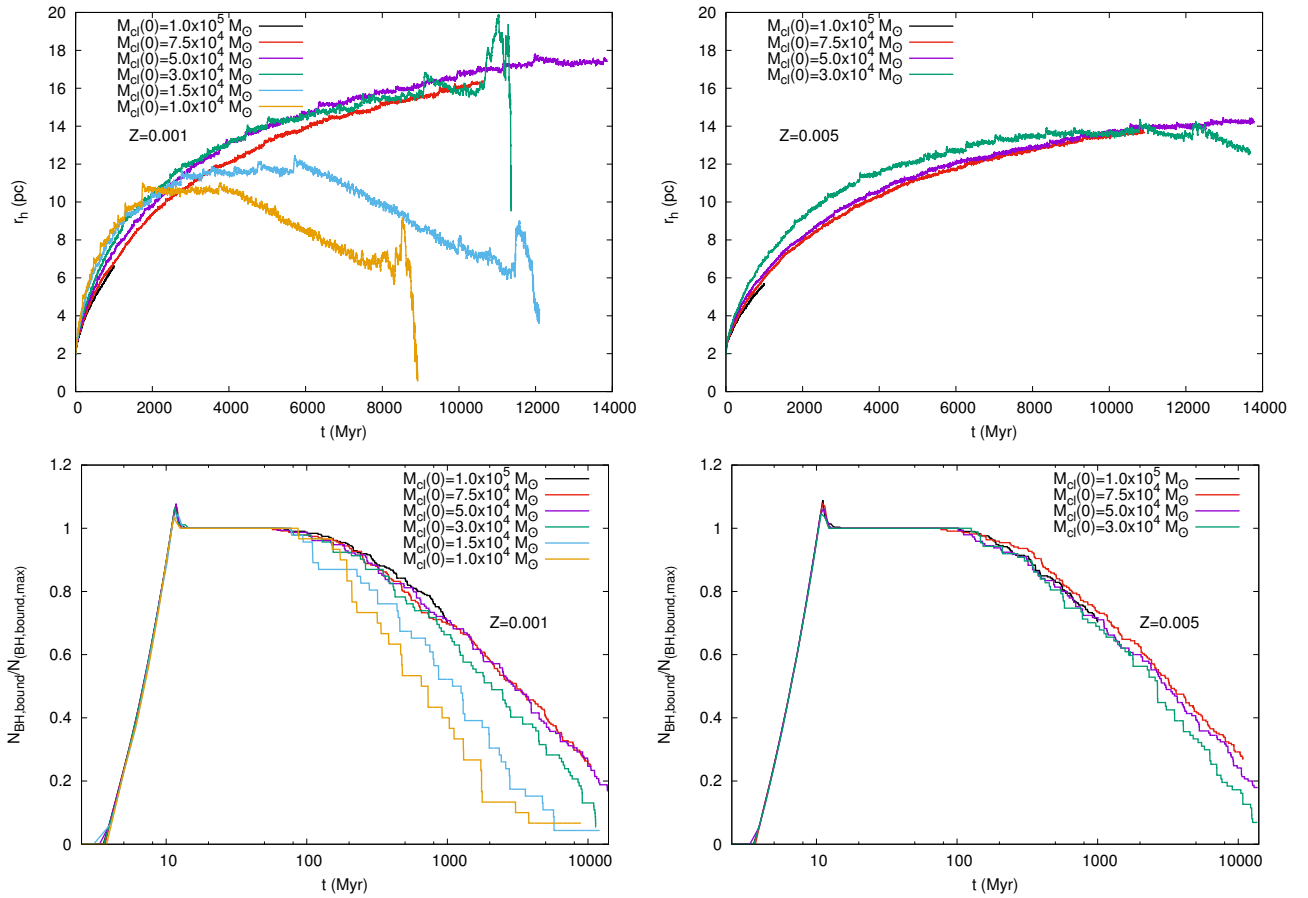


**Figure 2.** **Top panels:** The time evolution of the half-mass radius,  $r_h$ , for the computed initially single star-only models (see Table 1) with metallicities  $Z = 0.05Z_{\odot}$  (left) and  $0.25Z_{\odot}$  (right). **Bottom panels:** The time evolution of the fraction of BHs (normalized w.r.t. the number of BHs that initially remain bound to the cluster, *i.e.*, w.r.t. the flat part of the curves spanning between  $\approx 10 - \approx 100$  Myr) retaining in the models with these  $Z$ s.



age, are of sub- $Z_{\odot}$  (Harris 1996) or as parents of open clusters which are also often of sub- $Z_{\odot}$  (e.g., Heiter et al. 2014), in both Galactic and extragalactic environments. In any case, the computations here suggest that (Table 1, Secs. 2 & 3) the number of BBH mergers, for a given cluster, does not necessarily follow any systematics with the cluster’s metallicity ( $Z$ ) over a wide range; in fact higher- $Z$  clusters often produce as many or even more mergers than their lower- $Z$  counterparts. Therefore, the general conclusions from this work (Sec. 4) are likely to hold for clusters up to  $Z_{\odot}$  and hence in all types of hosts. The lower-mass YMCs and open-type clusters, as considered here, are as well interesting due to the fact that they comprise the vast majority of the dense stellar clusters and would potentially serve as a competent addendum to the GCs, in terms of their contributions to the dynamical BBH mergers (Sec. 3.3).

This paper is organized as follows. The newer cluster models with primordial binaries are introduced in Sec. 2, along with a brief description of the NBODY7 program in Sec. 2.1. The results from the computations are elaborated in Sec. 3: Sec. 3.1 discusses the dynamically-formed BBH mergers’ characteristics and their dependence on the parent cluster’s properties, Sec. 3.2 discusses the behaviour of the neutron stars in the presence of a dynamically-active population of BHs, and Sec. 3.3 discusses the contribution of young massive and open clusters to the dynamical BBH merger rate. Sec. 4 recapitulates the results.

## 2 MODEL CALCULATIONS: INTRODUCTION OF PRIMORDIAL BINARIES

Table 1 summarizes the new computations, as well as those from Paper I. Extending from Paper I, the newer models here *initiate* with Plummer profiles of masses  $M_{cl}(0) \approx 7.5 \times 10^4 M_{\odot}$  and  $1.0 \times 10^5 M_{\odot}$ , half-mass radius,  $r_h(0) \approx 2$  pc, and with only single stars. Since it takes much longer time to compute the  $M_{cl}(0) \approx 1.0 \times 10^5 M_{\odot}$  models, they are evolved only for  $T_{\text{evol}} \approx 1$  Gyr, as opposed to the long-term evolution for the rest of the models, but an additional metallicity of  $Z = 0.5Z_{\odot}$ , on the top of the metallicities  $Z = 0.25Z_{\odot}$  and  $0.05Z_{\odot}$ , are considered for the most massive models. As in Paper I, the zero-age main sequence (hereafter ZAMS) masses of the individual stars in all the newly computed models follow the standard Kroupa (2001) initial mass function (hereafter IMF), with the maximum stellar mass correlated with  $M_{cl}(0)$  (Weidner & Kroupa 2004; Kroupa et al. 2013).

In addition to the initially single star-only models, initially Plummer-profiled clusters of  $M_{cl}(0) \approx 3.0 \times 10^4 M_{\odot}$ ,  $r_h(0) \approx 2$  pc,  $Z = 0.25Z_{\odot}$  and  $0.05Z_{\odot}$ , and having a primordial-binary population are evolved for  $\approx 10$  Gyr. All YMCs, open clusters, and GCs are observed to contain a high to a small fraction of stars in hard (spectroscopic) binaries (Portegies Zwart et al. 2010). The inclusion of a primordial-binary population would not only make the models more realistic but would also potentially make the dynamical interactions richer and versatile, by virtue of the enhanced occasions of exchange interactions offered by the binaries. That way, they are likely to influence the formation of BBHs and other types of compact binaries, which effect has not yet been studied through detailed N-body simulations, especially, for massive and compact systems as in here.

While the inclusion of primordial binaries is intriguing, it also makes the computations more rigorous and time consuming, so that an economical strategy is adopted here for the computations with primordial binaries. First, a high primordial binary fraction of  $f_{\text{Obin}} \approx 100\%$  and the orbital period and eccentricity distributions of Sana & Evans (2011) are adopted for the O-type stars (ZAMS mass  $M_{\text{ZAMS}} \geq 16M_{\odot}$ ), to be consistent with the observed high (present-day) binary fractions among O-stars in YMCs, open clusters, and OB associations (Sana & Evans 2011; Sana et al. 2013; Oh et al. 2015). The binary mass ratios,  $q$ , among the O-type stars, follow a uniform distribution (here, an O-star is paired only with another O-star, as typically observed, and the pairing among the lower-mass stars is obtained separately; see below).

The binaries among stars with  $M_{\text{ZAMS}} < 16M_{\odot}$  are obtained separately, where much lower fractions of primordial binaries are adopted. The primary motivation for this is to reduce the computing cost; that way a low overall binary fraction can be maintained throughout the model’s evolution, easing the computing demand. For  $M_{\text{ZAMS}} < 16M_{\odot}$ , primordial binary fractions of  $f_{\text{bin}} \approx 2\%$ ,  $\approx 5\%$ , and  $\approx 10\%$  are taken (see Table 1), that cover the typical range of spectroscopic binary fractions in GCs and open clusters. Note that since, in all models, the O-type stars comprise only a small fraction of the total stellar population, the  $f_{\text{bin}}$  also represents the overall primordial binary fraction of the model, as opposed to the much higher  $f_{\text{Obin}} \approx 100\%$  primordial binary fraction among the O-stars themselves.

The orbital periods of the non-O-star primordial binaries are taken to follow a Duquennoy & Mayor (1991) distribution, and their eccentricities follow a thermal distribution (Spitzer 1987), that characterize a dynamically-processed binary population (Kroupa 1995a). Their mass ratios are taken to be uniform between  $0.1 \leq q \leq 1$ . It would, perhaps, have been more realistic to adopt a “birth” population of primordial binaries (Kroupa 1995a,b) or an analytically “pre-evolved” (primordial) binary population (Marks et al. 2011), but they would sustain a much higher binary fraction for the relatively modest  $M_{cl}(0) \approx 3.0 \times 10^4 M_{\odot}$ ,  $r_h(0) \approx 2.0$  pc clusters evolved here, making such long-term computations practically prohibitive. In that way, the present scheme of including primordial binaries provides a reasonable compromise between the economy of computing and consistencies with observations. Most importantly for this study, the progenitor stars of the BHs (i.e., the O-stars), in the primordial-binary models, begin in a more realistic environment comprising a high fraction of dynamically-active binaries, as observed (Sana & Evans 2011; Sana et al. 2013).

In fact,  $f_{\text{Obin}} \approx 100\%$  implies that the consequences of massive binary evolution is automatically taken into account (here, applying the binary-evolution routine BSE ; see below) but in their natural dynamically-active habitat, given that the majority of the massive stars and their binaries are observed to reside in dense stellar environments, as opposed to classical population-synthesis studies of compact-binary formation (see Sec. 1 and references therein) where the massive binaries are evolved without any external perturbation.

No primordial mass segregation is applied to the computed models in Table 1.

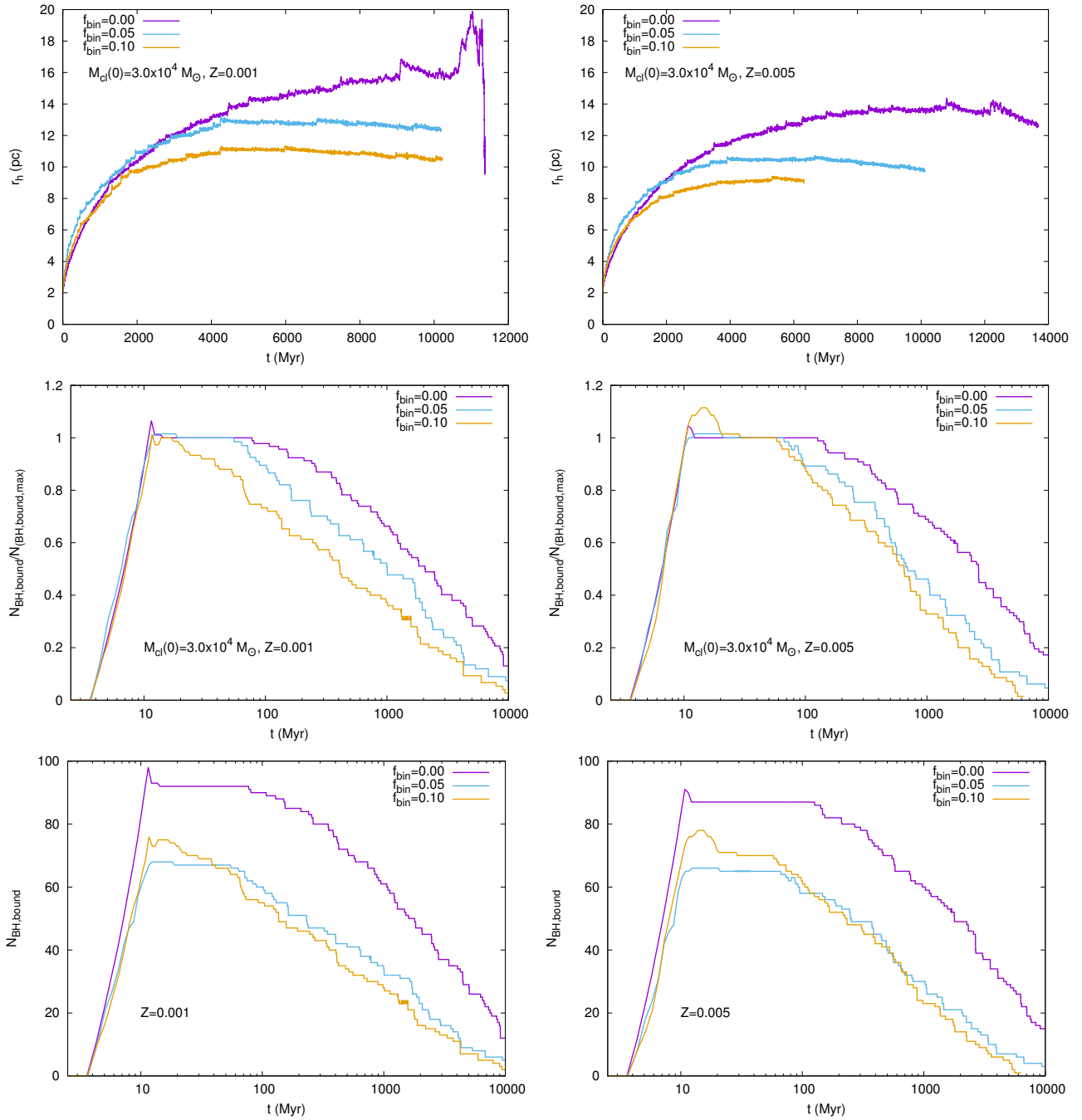


**Figure 3.** The time evolution of the half-mass radii (top panels), the retention fraction of BHs (middle), and the total number of bound BHs (bottom) for the computed models with initial masses  $M_{cl}(0) \approx 3.0 \times 10^4 M_{\odot}$ , metallicities  $Z = 0.05Z_{\odot}$  (left column) and  $0.25Z_{\odot}$  (right column), and overall primordial binary fractions  $f_{bin} \approx 0\%$ ,  $5\%$  and  $10\%$  (legends). These panels demonstrate that increasing the primordial binary fraction results in a general increase of the frequency of dynamical scattering interactions and energy injection, resulting in a faster decline of the cluster’s BH population and hence its approach towards core collapse.

## 2.1 The NBODY7 N-body evolution program

As in Paper I, all the newer computations here are carried out using the state-of-the-art direct N-body evolution program NBODY7<sup>1</sup> (Aarseth 2003, 2012, see also Rantala

et al. 2017); see Sec. 2.1 of Paper I for the details on this program. In short, it is a fourth-order Hermite integrator for tracking the individual trajectories in an arbitrary, self-gravitating, many-body system where the close encounters and the bound subsystems (binaries and multiples) are treated with regularization techniques. The integration is accelerated by utilizing a neighbour-based scheme (Nitadori & Aarseth 2012) for the force contributions at the short-

<sup>1</sup> In practice, NBODY7 and its predecessor NBODY6 (see below) are often used synonymously.

est time intervals (the “irregular” force/steps). At longer time intervals (the “regular” force/steps), all members in the system are included for the force evaluation. The irregular forces are computed by parallel processing in CPUs, while the much more expensive regular force evaluations are done on GPUs<sup>2</sup>. The diverging gravitational forces during close passages and in binaries are dealt with two-body or KS regularization (Aarseth 2003) and higher-order multiples are treated with the Algorithmic Regularization Chain (ARC; Mikkola & Tanikawa 1999; Mikkola & Aarseth 2002; Mikkola & Merritt 2008). Unlike the traditional- or KS-Chain Regularization (Mikkola & Aarseth 1993), that is utilized in NBODY6, the application of the ARC in NBODY7 allows the inclusion of members, in the Chain, with arbitrary mass ratios. This makes NBODY7 more suitable for the present calculations where the BHs are of a wide mass range and predominantly take part in binary-single and binary-binary interactions (see Sec. 1, below).

In NBODY7, the Chain members and the Chain perturbers are, however, selected in the same well-proven way as in the KS-Chain implementation in NBODY6 (Aarseth 2003, 2012), except that the internal integration of the Chain is done in the ARC way (Mikkola & Merritt 2008 and references therein). Here, the Chain members, that comprise a compact subsystem (often a triple or a quadruple), are initially selected based on the strategies for identifying hierarchical systems. This comprises identifying, for each particle in the system, the dominant and the next-to-dominant perturber and testing whether to form a triple or a quadruple; see Chapter 9 and Algorithm 11.3 of Aarseth (2003) for the details. The Chain is then constructed (and possibly switched during the Chain integration due to either change in the subsystem’s configuration or the close approach of a perturber) in the usual way by sequentially connecting the closest subsystem members with vectors as described in Mikkola & Aarseth (1993). The perturbers of the compact subsystem are selected either from within its close-encounter radius or otherwise through a full perturber search. The key algorithms are discussed in Chapter 12 of Aarseth (2003).

An important aspect of NBODY7 is its GR treatment of binaries and multiples containing a BH or a neutron star (hereafter NS), through the ARC<sup>3</sup> (Mikkola & Merritt 2008). This allows for on-the-fly GR orbital modifications and coalescences of relativistic subsystems (typically a binary or a triple containing one or more BH/NS) that are bound to the system. In principle, PN-1, PN-2 (GR periastron precession), PN-2.5 (orbital shrinking due to GW radiation), PN-3, and PN-3.5 order terms can be included in the ARC procedure, including their spin contributions. For the ease of computing, the PN orders are increased sequentially as they become significant; see Aarseth (2012) and references therein for the details of the implementation and Brem et al. (2013) for an alternative approach (in NBODY6++). However, for the economy in computing time, the BHs’ spins are taken to be zero in the present computations. The

spin terms would have modified the times of GR coalescences occurring within the cluster (see Secs. 1 & 3.1) to some extent, however, this is not critical here due to the statistical nature of the dynamically-induced BBH coalescences. The latest implementation shows reasonable energy check (typical relative energy change  $\sim 10^{-4} - 10^{-6}$ ) even during extreme relativistic events such as a BBH coalescence within a triple.

In reality when the BHs have spins, a BBH would typically receive a large GW merger kick during its inspiral phase ( $\sim 100 - 1000 \text{ km s}^{-1}$ ; Campanelli et al. 2007; Hughes 2009). This would cause the newly-formed merged BH to escape from the cluster almost immediately, and it would hardly have a chance to participate in dynamical encounters further. This situation is mimicked by applying a velocity kick onto the merged BH immediately after a GR BBH coalescence occurs within the cluster (Sec. 3.1). In the current implementation in NBODY7, the applied kick is kept only marginally above the escape speed to avoid large energy errors;  $\approx 5$  times the central RMS speed. This is still enough to eject the merged BH out of the cluster in several dynamical times; in reality a BBH coalescence product would typically escape at a much higher speed. In any case, it is found in test calculations that even if a merged BH is retained, it does not necessarily participate in further GR coalescences.

NBODY7 utilizes the semi-analytic single- and binary-stellar evolution algorithm BSE (Hurley et al. 2000, 2002) to evolve each star/binary and form their remnants (see Sec. 2.1 of Paper I). For comparison purposes, the same recipes of stellar evolution and remnant formation as in Paper I (see Sec. 2.2 of paper I) are adopted here for the newer computations. In brief, this involves a modified version of the BSE that adopts the state-of-the-art stellar-wind and remnant-formation schemes of Belczynski et al. (2008, 2010b), thereby allowing the formation of DCBHs and of NSs via electron-capture supernovae (ECS; Podsiadlowski et al. 2004), from both single stars and binary members. The DCBHs and the ECS-NSs are the massive-stellar remnants that receive zero natal kicks and are retained in the cluster at birth.

It is to be noted that the single-stellar BH mass spectrum (see Fig. 1 of Paper I and Fig. 1 here) gets modified when nearly all the BH progenitors are in binaries, as in the primordial-binary models here. This is due to the mergers of massive binaries or of binary components during binary-binary encounters, resulting in more massive progenitors and hence more massive BHs, and also due to the mass transfer, CE, and tidally-enhanced stellar winds that might occur within the binaries, modifying the components’ mass evolution. The BH masses are likely to be as well different from those in a pure population synthesis approach (for given stellar- and binary-evolution schemes; here the modified BSE) since the stochastic dynamical perturbations and close interactions would modify the binaries’ evolutions. The mergers among the massive primordial binaries would also cause less number of DCBHs (but with a broader mass spectrum) to be produced compared to the initially single-only counterpart; see the bottom panels of Fig. 3. Fig. 1 demonstrates the difference in the BH mass spectra in the two cases for the  $M_{cl}(0) \approx 3.0 \times 10^4 M_{\odot}$  models; the distributions here correspond to an early evolutionary time of  $t \approx 20 \text{ Myr}$  and include the non-DCBHs too, that would escape soon after

<sup>2</sup> All computations in this work are done on workstations equipped with quad-core AMD processors and NVIDIA’s Fermi and Kepler series GPUs.

<sup>3</sup> To accommodate the unlikely event of a pure KS binary becoming relativistic, GR orbital modifications are included in the KS treatment as well.

due to their natal kicks, although there are only a handful of such BHs per cluster for the  $Z \leq 0.25Z_{\odot}$  considered here.

### 3 RESULTS

Fig. 2 compares the time evolution of the half-mass radius,  $r_h(t)$ , and of the fraction of the bound BHs, for the initially single star-only models in Table 1. As already noted in Paper I (see its Sec. 3.1), for a given initial size  $r_h(0) \approx 2$  pc and a given  $Z$  (BH mass spectrum), the dynamical heating of the BHs begins to expand an initially less massive (dense) cluster at a somewhat larger rate. However, in the long run, more numerous BHs in a higher  $M_{cl}(0)$  system continue to expand their host for a longer time, that, in turn, inhibits the dynamical self depletion of the BHs, ultimately continuing to retain a larger fraction of the initially-bound BHs (*c.f.* Fig. 5 of Paper I). As pointed out in Sec. 1, such self-regulation is responsible for the long-term retention of BH populations, especially in massive low- $Z$  systems such as GCs, where stellar-mass BH candidates have recently been identified.

Fig. 3 compares the evolution of the size and the BH retention fraction among the  $M_{cl}(0) \approx 3.0 \times 10^4 M_{\odot}$  models with and without primordial binaries (see Table 1). Interestingly, the BHs deplete faster, in long term, in the presence of a higher primordial binary fraction (Fig. 3, middle panels). This is a consequence of the overall increase in the rate of strong scattering encounters, with increasing primordial binary fraction (among the lower-mass stars; see Sec. 2), that the BHs experience while they continue to interact with the other stellar members of the cluster (see Sec. 1). The correspondingly enhanced rate of BH loss, in turn, stalls the expansion of the cluster and resumes its secular contraction (Spitzer 1987) earlier (Fig. 3, top panels). The presence of primordial binaries, therefore, might be the key to prevent old, low- $Z$  GCs to grow to unusually large sizes (*c.f.* , Morscher et al. 2015; Chatterjee et al. 2017a).

#### 3.1 Dynamically-formed BBH: gravitational-wave coalescence events

The sixth (seventh) column of Table 1 enlists the individual BBH coalescences that occur while being bound to the cluster (occur within a Hubble time after being ejected from the cluster), where the merging masses ( $M_{BH1} + M_{BH2}$ ) and the corresponding cluster-evolutionary times<sup>4</sup> for the merger (ejection),  $t_{\text{mrg}}(t_{\text{ej}})$ <sup>5</sup>, are provided in the parentheses. As already seen in Paper I, the BBH coalescences<sup>6</sup>, in these models, occur predominantly while being bound to the cluster, rather than happening among those BBHs that are ejected from the cluster. As discussed in Sec. 3.2 of Paper I, this is expected for the lower-mass, open-type clusters, as simulated here, in the presence of a broad BH mass spectrum,

as obtained from the present remnant-formation schemes. Such in-cluster or in situ BBH mergers are typically induced via large eccentricity boost of the merging BBH, while it is a part of a triple (with typically a BH or possibly with a normal stellar member), due to the triple’s internal dynamical evolution. Such triples continue to form and disassemble due to the numerous close encounters involving single BHs, BBHs and/or normal stellar binaries (see Sec. 1 and references therein).

In fact, as apparent from Table 1, the number of such triple-mediated BBH mergers, in general, increase dramatically in the presence of primordial binaries; *c.f.* the  $M_{cl}(0) \approx 3.0 \times 10^4 M_{\odot}$  models in Table 1 with  $f_{\text{bin}} = 0$  and  $f_{\text{bin}} > 0$ . Like the enhanced depletion rate of the BHs (see above; Fig. 3), this is also a consequence of the persistent population of (lower-mass) primordial binaries being continuously engaged in close encounters with the BHs, thus allowing additional BBH formation via exchange encounters. An increase of the number of in situ BBH mergers, with the overall binary fraction, can also be noted in the much more massive clusters in Monte Carlo-based studies, *e.g.*, in Morscher et al. (2015). In fact, all the in situ BBH coalescences in the primordial-binary models here involve BHs from different primordial binaries, *i.e.*, all of them are assembled through exchange interactions. For the  $f_{\text{bin}} > 0.05$  clusters, 10-20% of the *ejected* BBHs, per model, contain BH members that are derived from the same primordial binary.

As an inspection of the current computation outputs reveals, the majority of the BBH inspirals occur in triples that are intermediate or metastable in nature (Sec. 1 and references therein). However, although rare, cases are spotted where a highly hierarchical and long-lasting triple has ultimately led to the GR inspiral and merger of its inner BBH through the eccentric Kozai mechanism, in its regular sense (Sec. 1 and references therein). Note that hierarchical triples, in dense systems such as here, are often perturbed by intruders so that their evolutionary and stability properties differ from those had they evolved in isolation. A more thorough study of the nature of the (resonant/hierarchical) triples/multiples hosting a BBH merger, in realistic cluster environments as here, is currently ongoing (Banerjee, in preparation). In the rest of this paper, the in-cluster GR mergers will simply be denoted as “triple-induced mergers”.

In contrast, Monte Carlo simulations of much more massive, GC-like clusters, typically of  $10^5 M_{\odot} \lesssim M_{cl}(0) \lesssim 10^6 M_{\odot}$  (see Sec. 1 and references therein), predominantly yield ejected BBH mergers. Such massive systems, typically unapproachable by the direct N-body method (but see Wang et al. 2016; Sec. 1), eject BBHs that are much tighter, owing to the clusters’ large escape speeds, facilitating mergers among them, unlike those here. It should, however, be noted that a direct N-body approach, with explicit GR treatment, deals with subsystems more consistently and completely than in a typical Monte Carlo approach (see Sec. 1 and references therein); the former approach would perhaps inherently (and more realistically) lead to a larger number of on-the-fly, triple-induced GR coalescences than its Monte Carlo counterpart. At present, the ranges of models computed with the two techniques by different groups and the details of the dynamical treatments adopted in them barely overlap. This makes a direct comparison among the two regimes and the methods, especially in terms of rare strong-

<sup>4</sup> Unless otherwise stated, all merger times,  $t_{\text{mrg}}$ , are measured w.r.t. the beginning of the parent cluster’s evolution.

<sup>5</sup> The instant of ejection of any entity is taken as the time at which it crosses the tidal radius.

<sup>6</sup> In NBODY7, the speed of light can be “chosen” so as to make the system more or less relativistic. In all the computations presented here, the physical speed of light is always chosen.



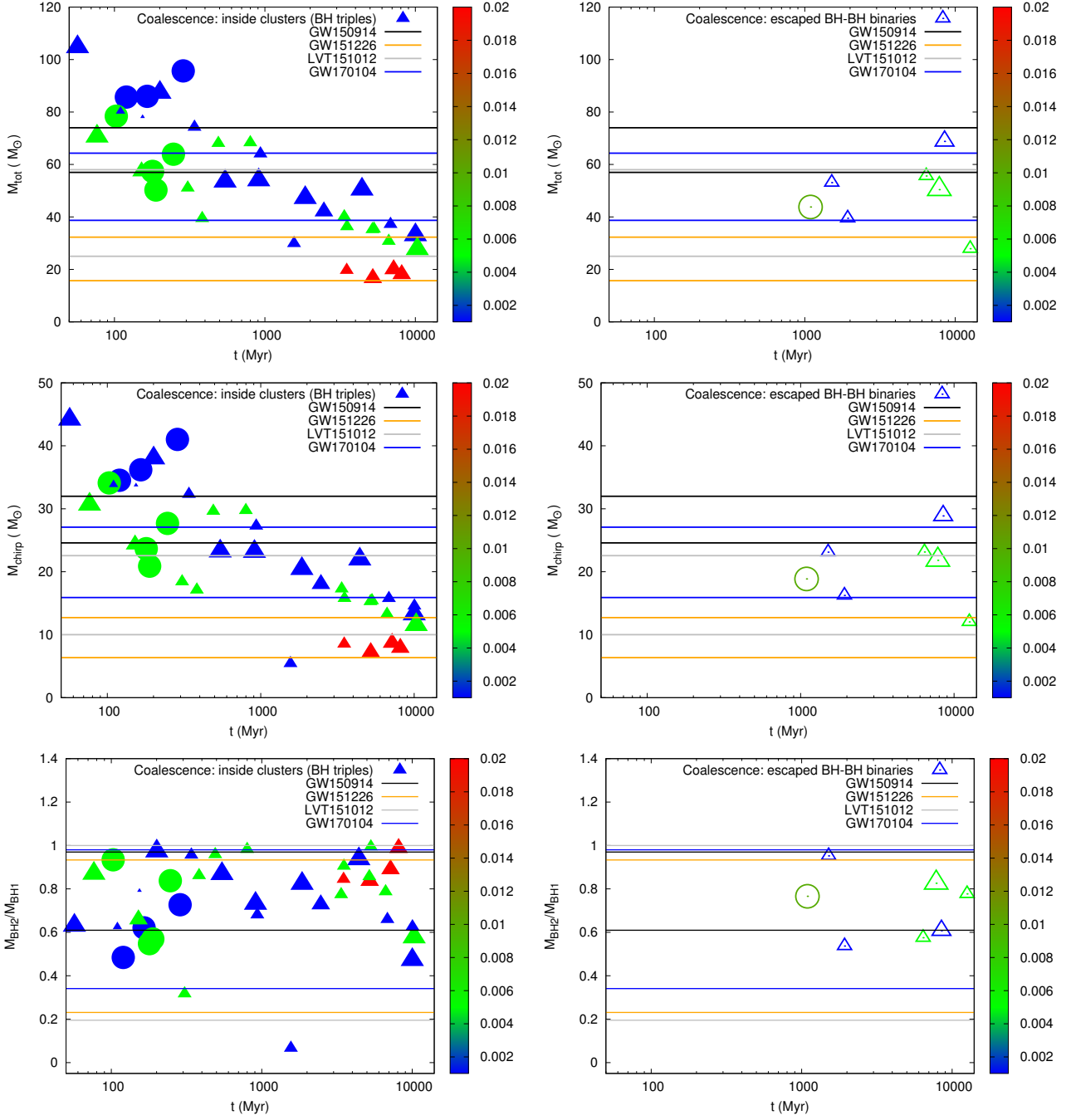


**Figure 4.** **Left column:** The total mass,  $M_{\text{tot}}$  (top panel), chirp mass,  $M_{\text{chirp}}$  (middle), and the mass ratio,  $M_{\text{BH2}}/M_{\text{BH1}}$  ( $M_{\text{BH2}} \leq M_{\text{BH1}}$ ; bottom), of the (triple-mediated) BBH coalescences that occur while being bound to the clusters, against the cluster-evolutionary times,  $t = t_{\text{mrg}}$ , at which the mergers occur. The mergers for all models with initial masses  $M_{\text{cl}}(0) \lesssim 7.5 \times 10^4 M_{\odot}$  (see Table 1) are represented by filled triangles whose sizes are scaled in proportion to the clusters'  $M_{\text{cl}}(0)$ s and which are colour coded according to the models' assumed metallicities (the colour bars; Table 1). The mergers within the  $M_{\text{cl}}(0) \approx 10^5 M_{\odot}$  models are denoted by filled circles which have the same colour coding. The particular coalescence with mass ratio  $\approx 0.1$  (see bottom panel) is actually an NS-BH merger. **Right column:** The same as the left column but for the coalescences, occurring within the Hubble time, among the BBHs that are ejected from the clusters and for the mergers being represented by the corresponding empty symbols. Here, the plotted merger times,  $t = t_{\text{mrg}}$ , include the cluster-evolutionary times,  $t_{\text{ej}}$ , of the BBHs' ejections, *i.e.*,  $t_{\text{mrg}} \equiv t_{\text{ej}} + \tau_{\text{mrg}}$ , where  $\tau_{\text{mrg}}$  is the GW merger time (Peters 1964) of the BBH right after its ejection.

encounter products such as dynamical BBH mergers, difficult. However, in terms of the overall long-term behaviour of the clusters, Monte Carlo and direct N-body approaches have shown to yield mutually agreeable outcomes (see, *e.g.*, Giersz et al. 2013; Rodriguez et al. 2016b).

The left (right) column of Fig. 4 shows the triple-induced (ejected) BBH mergers' total mass,  $M_{\text{tot}}$ , chirp mass,  $M_{\text{chirp}}$ <sup>7</sup>, and mass ratio,  $M_{\text{BH2}}/M_{\text{BH1}}$  ( $M_{\text{BH2}} < M_{\text{BH1}}$ ), against their respective merger times,  $t = t_{\text{mrg}}$ , where the outcomes of all the models in Table 1 are superimposed. A clear negative trend is visible between the *bound* BBH mergers'  $M_{\text{tot}}$  or  $M_{\text{chirp}}$  and their  $t_{\text{mrg}}$ s (Fig. 4, left column): this is simply due to the fact that the more massive BHs remain more centrally concentrated and hence predominantly get engaged in dynamical interactions, at earlier evolutionary times. Such a behaviour is also seen in the merger times of *ejected* BBHs from massive GCs; see, *e.g.*, Chatterjee et al. (2017b).

On the other hand, in the present computations, no clear trend between the  $t_{\text{mrg}}$ s and the masses is apparent for the ejected BBHs (Fig. 4, right column). First, there are only a few ejected BBHs with  $t_{\text{mrg}} < 13.7$  Gyr. A trend is furthermore washed out due to the fact that the occurrence of a merger within a Hubble time, for these relatively wide (semi-major-axis =  $a$ ), ejected BBHs, relies mostly on their dynamically-induced, very high (initial) eccentricities,  $e$ , which sensitively controls the binaries' GR coalescence time,  $\tau_{\text{mrg}}$ , through (Peters 1964)

$$\tau_{\text{mrg}} \approx \frac{5}{64} \frac{c^5 a^4 (1-e^2)^{7/2}}{G^3 m_1 m_2 (m_1 + m_2)} \left( 1 + \frac{73}{24} e^2 + \frac{37}{96} e^4 \right)^{-1}, \quad (1)$$

where  $m_1 = M_{\text{BH1}}$  and  $m_2 = M_{\text{BH2}}$  are the members' masses of the BBH<sup>8</sup>.

Fig. 5 (left panel) demonstrates the overall negative trend of the  $M_{\text{tot}}$ s of the ejected BBHs w.r.t. their  $t_{\text{ej}}$ s, as for the in situ BBH coalescences (see above; Fig. 4). The formation of higher-mass BHs in the models with primordial binaries (see Sec. 2.1; Fig. 1) results in the ejection of more massive BBHs from such models, especially at early evolutionary times. Higher  $M_{\text{cl}}(0)$  models generally tend to eject tighter BBHs (with shorter orbital periods), owing to larger escape speeds from their centers. The orbital periods,  $P$ , of the ejected BBHs have an overall positive correlation (despite large scatter) with  $t_{\text{ej}}$ : this is due to the expansion and mass loss of the clusters with time (see above), diluting their central potentials and correspondingly reducing their escape speeds. These trends are demonstrated in Fig. 5 (right panel; see also Chatterjee et al. 2017a). Note that the ejected BBHs with the smallest  $P$ s are generally moderately eccentric (see colour coding in Fig. 5), so that such systems with  $\tau_{\text{mrg}} < 13.7$  Gyr are rare, for the cluster mass range explored here.

<sup>7</sup> The chirp mass between two masses  $m_1$  and  $m_2$  is defined as  $M_{\text{chirp}} \equiv \frac{(m_1 m_2)^{3/5}}{(m_1 + m_2)^{1/5}}$ .

<sup>8</sup> Note that Eqn. 1, which is used in plotting the data points in the right panels of Fig. 4, is an approximate formula that, depending on the initial  $e$ , underestimates  $\tau_{\text{mrg}}$ . A more accurate value of  $\tau_{\text{mrg}}$  can be obtained by explicitly integrating the Peters (1964) expressions of (orbit-averaged)  $a$  and  $e$  decay, as done in Sec. 3.1.1. The sensitive dependence of the  $\tau_{\text{mrg}}$  of the inspiral on the initial  $e$  remains as well valid in the more accurate treatment.

Also, due to the enhanced rate of scattering and exchange encounters (see above), the ejected BBHs from the  $f_{\text{bin}} > 0$  models are more numerous compared to those from their  $f_{\text{bin}} = 0$  counterparts (open squares in Fig. 5).

As hinted in Paper I, although dynamical selection tends to pair BHs of similar masses (see Sec. 3.2 of Paper I), the mass ratios of the BBH mergers (both the bound and the ejected ones) would still have a rather broad range, typically  $0.5 \leq M_{\text{BH2}}/M_{\text{BH1}} \leq 1.0$ . This is demonstrated in Fig. 4 (bottom panels); the one with the mass ratio  $\approx 0.1$  is actually an NS-BH merger (see Sec. 3.2). Fig. 6 demonstrates that the distribution of the mass ratios of the BBH mergers, for  $M_{\text{BH2}}/M_{\text{BH1}} \gtrsim 0.5$ , is approximately flat except for the spike at  $M_{\text{BH2}}/M_{\text{BH1}} \approx 1.0$ . On the other hand, the BBH formation and coalescence channels involving purely massive binary evolution tend to produce BBHs and their mergers with mass ratios, typically,  $M_{\text{BH2}}/M_{\text{BH1}} \gtrsim 0.7$  (*e.g.*, Marchant et al. 2016; Belczynski et al. 2016). However, Belczynski et al. (2017) have recently produced a wider range of BBH-merger mass ratio, with modified input physics. Hence, a mass ratio substantially less than unity (as in GW151226 and GW170104 events) can be taken as an indication of the involvement of dynamical encounters in assembling a BBH merger, besides, any spin-orbit misalignment (see Sec. 1).

The limits of  $M_{\text{tot}}$ ,  $M_{\text{chirp}}$ , and  $M_{\text{BH2}}/M_{\text{BH1}}$ , for the events detected so far by the LIGO, are indicated in the panels of Fig. 4, where the data-points generally conform with these limits. Among the triple-induced (in situ) mergers occurring within a few 100 Myr of the parent cluster's evolution (Fig. 4, left panels), there are ones that are significantly more massive than even the most massive detected merger, namely GW150914. In terms of  $M_{\text{tot}}$  or  $M_{\text{chirp}}$ , the computed clusters typically generate GW150914-like and super-GW150914 mergers within them during their YMC phase ( $t \sim 10 - 100$  Myr), GW150914-like, GW170104-like, and GW151226-like mergers during their intermediate ages ( $t \sim$  Gyr), and only GW151226-like mergers are produced within the clusters from intermediate age onwards. Note that GW170104-like mergers are produced (within the low- $Z$  clusters) over the widest age range of the host clusters, from the YMC phase until nearly 10 Gyr age. In all the models computed here, all types of *ejected* BBH mergers take place from the clusters' intermediate age onwards (Fig. 4, right panels).

### 3.1.1 Binary black hole inspirals in the computed models

Nearly all BBH inspirals in the present models, be it triple-induced or ejected, begin with very high eccentricities, that ensure their short coalescence times (Eqn. 1). For the triple-induced (bound) cases, the resonant interaction/Kozai mechanism (Sec. 1) induces a high eccentricity in the inner BBH and, in the ejected BBHs, the high eccentricities are due to their internal orbital modifications by the close encounters that ejected them. While a high  $e$  ensures short  $\tau_{\text{mrg}}$  or at least  $\tau_{\text{mrg}} < \text{Hubble time}$ , it also raises the question whether a detectable eccentricity remains when the inspiralling BBH emits GW within, say, the LIGO's detection band or whether such eccentric BBHs will be audible (as persistent sources) by the future space-based GW observatories like the Laser Interferometer Space Antenna (hereafter LISA; Amaro-Seoane et al. 2017).

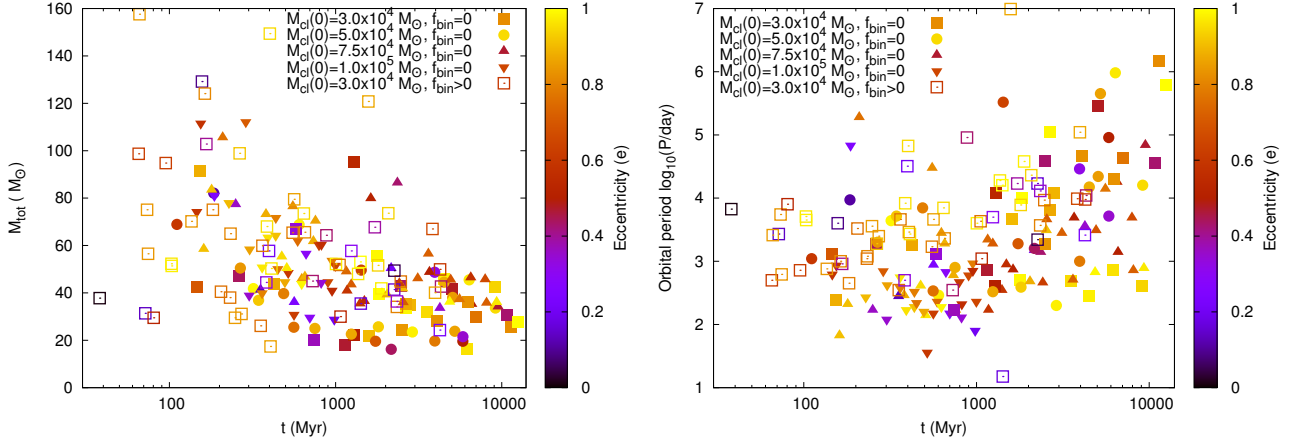


**Figure 5.** The ejected BBHs from all the  $M_{cl}(0) \geq 3.0 \times 10^4 M_\odot$  models in Table 1. The BBH data points are distinguished w.r.t. their parent clusters'  $M_{cl}(0)$  and primordial-binary content (legends) and are colour-coded w.r.t. their eccentricities,  $e$ , at the instant of ejection (colour bars). The total masses,  $M_{tot}$ s, of the BBHs show an overall decreasing trend w.r.t. their cluster-evolutionary times,  $t = t_{ej}$ , of ejection (left panel) and their orbital periods,  $P$ , at the instant of ejection, show an increasing trend (right panel). These trends qualitatively conform to what can be expected from the secular dynamical evolution of the clusters; see text.

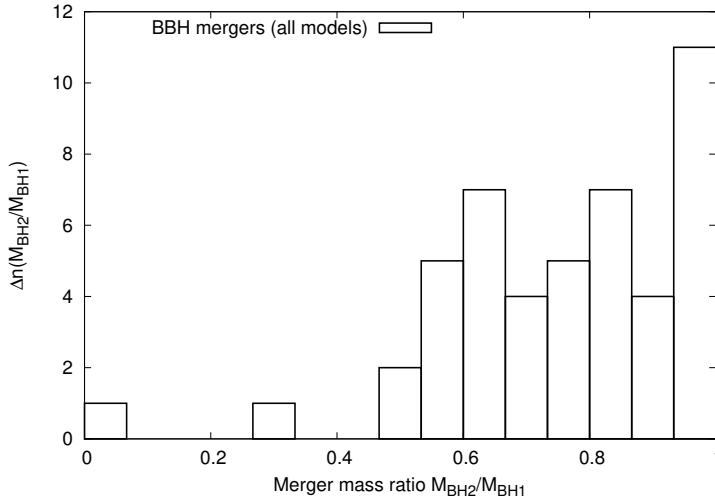


**Figure 6.** The distribution of mass ratios,  $M_{BH2}/M_{BH1}$ , of the BBH mergers from all of the models in Table 1 combined (includes both the in situ and escaped mergers). The distribution is approximately flat for  $M_{BH2}/M_{BH1} \gtrsim 0.5$  with a peak at  $M_{BH2}/M_{BH1} \approx 1$ . The merger with the lowest mass ratio is an NS-BH merger (see Fig. 4, Sec. 3.2).

The GW radiated by an eccentric binary is broadband whose peak frequency is given by (Wen 2003)

$$f_{\text{GWP}} = \frac{\sqrt{G(m_1 + m_2)}}{\pi} \frac{(1 + e)^{1.1954}}{[a(1 - e^2)]^{1.5}}. \quad (2)$$

Fig. 7 (top panel) shows the trajectories, in the  $\log_{10}(e)$ – $\log_{10}(f_{\text{GWP}})$  plane, of the in-spiralling inner BBHs of the BH triples, that have merged while being bound to the clusters in Table 1 (see its column ‘f’). At this stage, the GW radiation timescale of the inner BBH is much shorter compared to the Kozai/dynamical timescale of the associated triple (as indicated by the ARC treatment; see Sec. 2.1 and references therein), making the GR coalescence unavoidable. These tracks are obtained by integrating the Peters (1964) GR semi-major-axis and eccentricity decay formulae, beginning with the orbital parameters of the merging BBHs that

are logged by NBODY7 in its GR coalescence events’ records<sup>9</sup>. For most of these BBHs, when they have high eccentricities they emit GW with  $f_{\text{GWP}}$  either within the LISA’s characteristic detection frequency band or within the deciHertz range (see Fig. 7, top panel). Most of the BBHs which initially emit in the LISA band, circularize sufficiently while traversing through the same band so that they eventually become audible by the LISA (when  $e \lesssim 0.7$ ; see, e.g., Chen & Amaro-Seoane 2017) and their remaining eccentricities would then

<sup>9</sup> A better way to obtain such trajectories of triple-induced GR inspirals would be to allow for an on-the-fly, high-time resolution output of the orbit of a BBH during its GR inspiral, from within NBODY7, which is planned in a future paper. That way, any modifications of the orbital decay due to the perturbations from the third body could also be tracked.

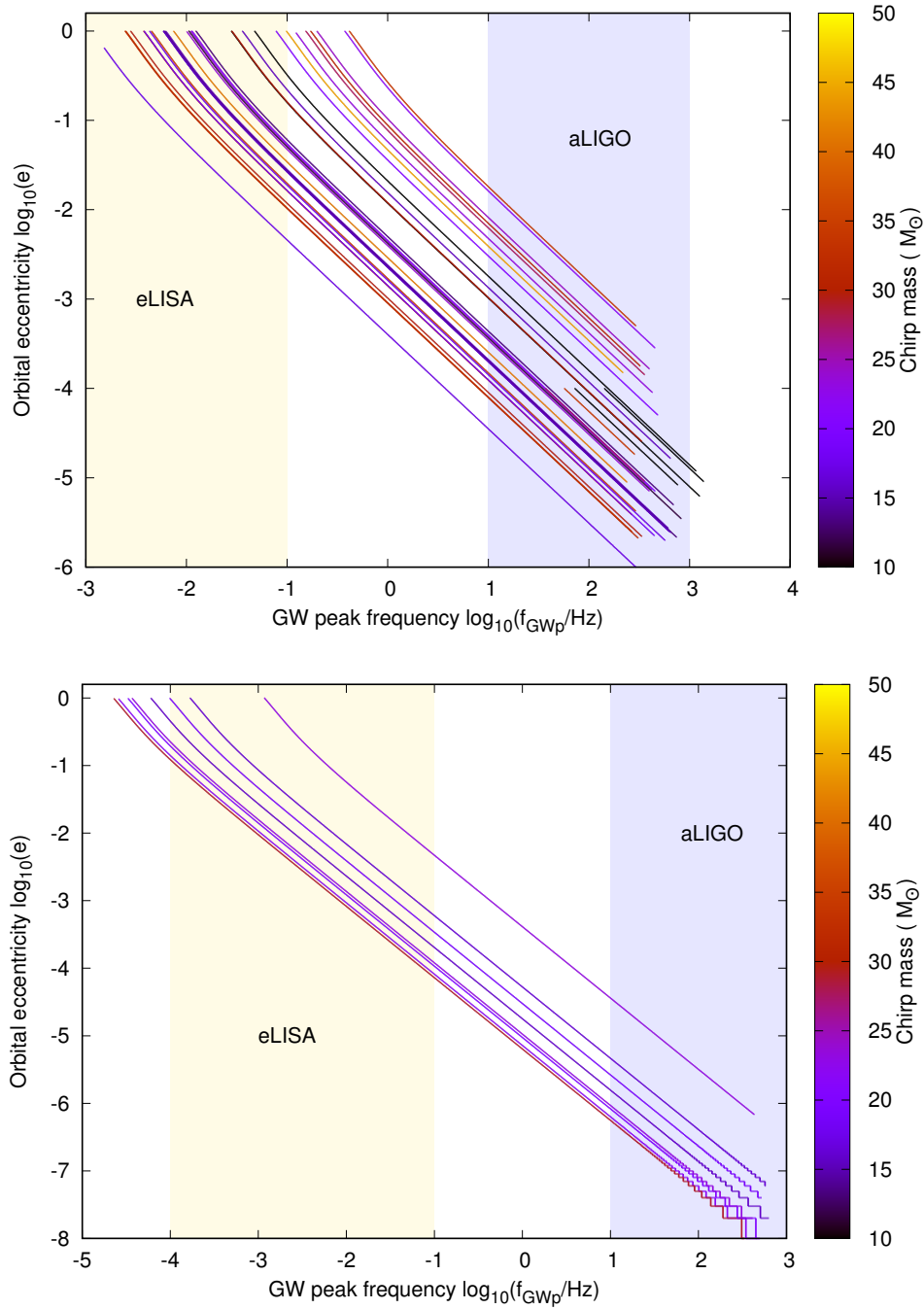


**Figure 7. Top:** Final orbital inspiral curves of the coalescing BBHs, that are bound to the clusters, in the  $\log_{10}(e) - \log_{10}(f_{\text{GWp}})$  plane,  $e$  being the BBH's eccentricity and  $f_{\text{GWp}}$  being the GW frequency at the peak of the BBH's GW power spectrum (see text). The gold and the blue shades represent the characteristic detection frequency bands of the LISA and the LIGO instruments. The curves are obtained by integrating the Peters (1964) orbit-averaged semi-major-axis and eccentricity decay formulae, initiating with the BBH parameters in the coalescence event record. They are colour coded according to the corresponding BBH's chirp mass. These curves suggest that although they begin spiralling in due to very high eccentricities (driven by resonant triples/Kozai mechanism; see text), the BBHs typically become sufficiently circular to be detectable by the LISA (see text) whilst traversing the instrument's frequency band and become nearly circularized by the time they enter the LIGO's frequency band. **Bottom:** The same, for the ejected BBHs that coalesce within a Hubble time and a similar description applies to them; they acquire the high eccentricities, at the beginning of their in-spiral, due to the close dynamical encounters that have led to their ejections.



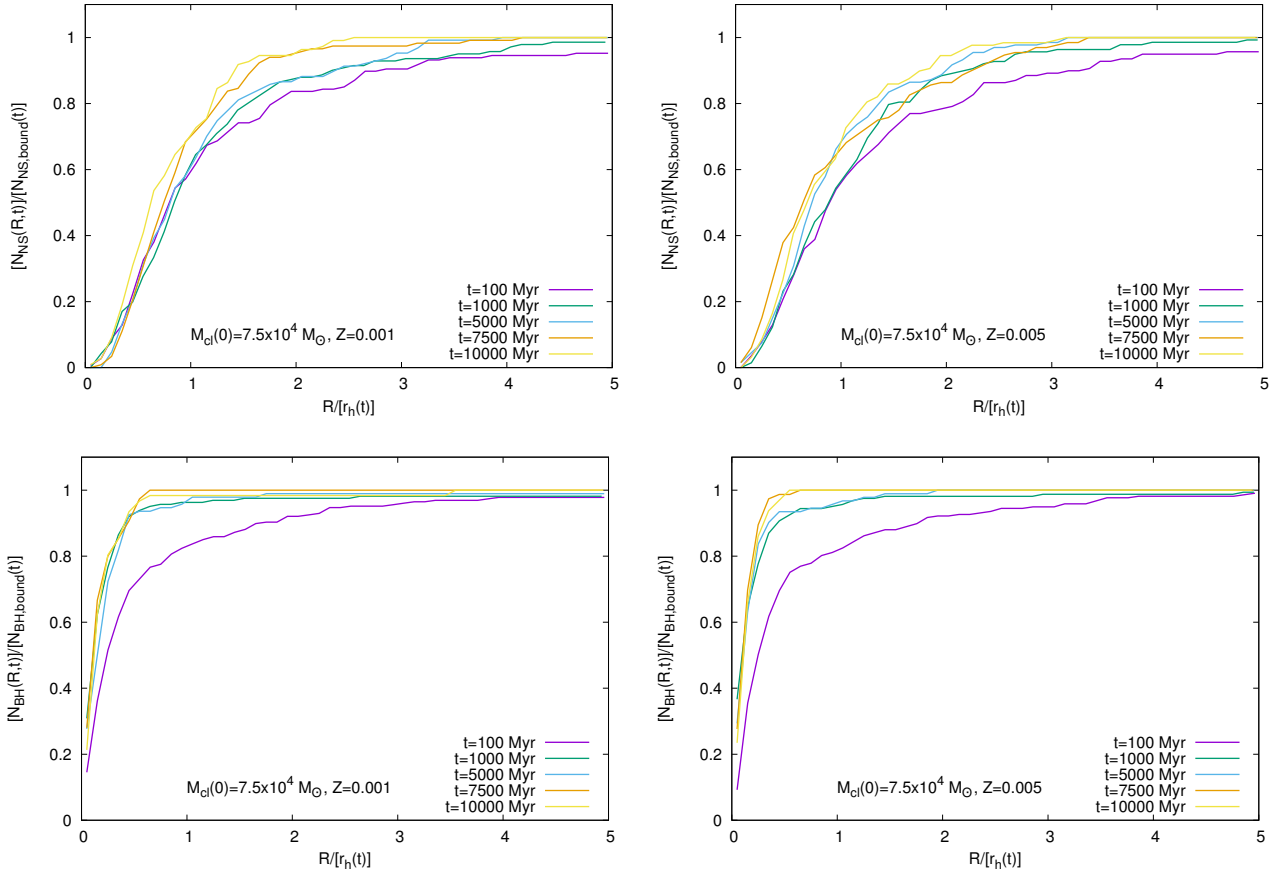


**Figure 8. Top:** The cumulative radial distribution of the (bound) NSs, at increasing evolutionary times (legends), for the  $M_{cl}(0) \approx 7.5 \times 10^4 M_{\odot}$  computed models (Table 1). The number of NSs,  $N_{NS}(R, t)$ , within a radial distance,  $R$ , and at an evolutionary time,  $t$ , is normalized w.r.t. the total number of NSs,  $N_{NS, bound}(t)$ , bound to the cluster at that time and the radial axis is normalized w.r.t. the cluster’s half-mass radius,  $r_h(t)$ , at time  $t$ . These cumulative distributions imply that although the NSs continue to centrally segregate with time, the mass segregation is inefficient due to the dynamical energy injection by the BHs, as already indicated in Banerjee (2017) — at late evolutionary times,  $\approx 90\%$  of the NSs occupy 2 half-mass radii. **Bottom:** The same treatment as in the top panels but for the BHs bound to the clusters. They imply that, except for very early evolutionary times, the much more massive BHs are generally much more strongly centrally concentrated than the NSs, as can be expected — nearly all BHs are contained within one half-mass radius.

serve as signatures of their dynamical origin (Nishizawa et al. 2016, 2017). By the time the BBHs spiral in to emit (in terms of  $f_{GWp}$ ) within the LIGO’s characteristic detection frequency band, they are practically circularized; the most eccentric BBHs in the LIGO band have  $10^{-2} < e < 10^{-1}$ . For all these BBHs, the time spent in the plotted trajectories until merger vary from a few years to  $\approx 0.1$  Myr. Hence, some of these BBHs would qualify for the combined LISA-LIGO detectability (Sesana 2016).

Fig. 7 (bottom panel) shows such tracks for the escaped BBHs with  $\tau_{mrg} < 13.7$  Gyr, from all the computed clusters in Table 1 (see its column ‘g’). As in the panel above, these tracks are obtained by integrating the Peters (1964) formulae, initiating with the orbital parameters of these BBHs at the instants of their ejections (as logged by NBODY7). All of these BBHs are ejected with very high eccentricities (which is why they have shorter  $\tau_{mrg}$ ; see Eqn. 1) when their  $f_{GWp}$ s lie within or below the LISA’s detection band. As in the case of triple-induced mergers (see above), these BBHs circularize sufficiently to be heard by the LISA while traversing

through the instrument’s detection band and are practically circularized when they enter the LIGO’s detection band.

Studies such as Samsing et al. (2014); Samsing & Ramirez-Ruiz (2017); Antonini et al. (2014, 2016, 2017) suggest the occurrences of BBH mergers that retain significant eccentricities,  $e > 0.1$ , in the LIGO band ( $f_{GWp} \geq 10$  Hz); matching with the corresponding GW waveforms would require GW templates from eccentric binaries (Huerta & Brown 2013). In the latter three studies, the same ARC code as here (Sec. 2.1) has been applied to directly integrate the (isolated/field) triple BHs. Note that the GC- or nucleus-type model clusters, that are considered as the hosts/parents of the triple-BHs/ejected-BBHs in the above works, are about an order of magnitude more massive than the present open cluster-type models. Therefore, the former clusters would contain tighter BBHs that can become members of triples or be ejected, with higher probabilities of retaining higher eccentricities in the LIGO band. With a larger model set giving a larger sample of triple-induced and ejected BBH mergers, such “eccentric” LIGO mergers can, perhaps, be obtained in similar models.

### 3.2 Properties of the neutron star population: mass segregation and neutron star binaries

The sustained energy injection by the BHs modifies the standard two-body relaxation driven processes in the cluster such as its approach towards core collapse and mass segregation. In particular, as demonstrated in Paper I, the presence of the BHs would keep the NSs from undergoing mass segregation significantly and thus from becoming a subpopulation that, like the BHs, would control the dynamics of the cluster and form relativistic subsystems efficiently (see Figs. 6 & 7 of Paper I and the corresponding discussions therein). Fig. 8 (top panels) illustrates this explicitly with the  $M_{cl}(0) \approx 7.5 \times 10^4 M_\odot$  models; w.r.t. the cluster's (time-varying) half-mass radius,  $r_h(t)$ , the NSs' central concentration increases only moderately with time. At the latest evolutionary times, the NSs occupy the volume engulfed by  $R = 3r_h(t)$  with  $\approx 90\%$  of the NSs lying within  $R < 2r_h(t)$ . In contrast, except for the earliest evolutionary times when it is still in the midst of mass segregation, the bulk of the BHs always remains concentrated well within  $r_h(t)$  (Fig. 8, bottom panels). Similar descriptions are valid for the long-term evolution of the NSs' radial distribution for the other lower-mass models in Table 1, as illustrated in Fig. 9; this figure also demonstrates that the more efficient ejection of the BHs from the clusters with primordial binaries allows a marginally higher degree of segregation of the NSs in them (the black lines in Fig. 9).

Notably, the majority of the NSs in GCs are found well within the clusters' half-mass radii (see, *e.g.*, Ransom 2008a,b; Hut & Verbunt 1983), unlike what is derived here. This may not, however, represent a discrepancy since such pulsar surveys in GCs are unlikely to reveal the complete NS populations and could be biased towards the clusters' innermost regions where the NSs' spatial densities are still the highest. A direct comparison, in this respect, between the present models and much more massive GCs would not hold; a much higher stellar density and hence stronger dynamical friction in GCs would aid the NSs' segregation, resulting in more centrally-concentrated NS profiles.

The present  $f_{\text{bin}} > 0$  models in Table 1 are found to produce any hard double neutron star (hereafter DNS) binary<sup>10</sup> neither through dynamical means nor through the evolution of massive (dynamically-active; see Sec. 2.1) primordial binaries. Note that although the formation of DNSs through the former channel depends on the extent of the NSs' dynamical activity, which, in turn, depends on how well concentrated they are, the latter channel always have the potential to give rise to DNSs in stellar clusters (see, *e.g.*, Belczynski et al. 2002; Lorimer 2008; Belczynski et al. 2010a; Ośłowski et al. 2011; Tauris et al. 2017). The non-occurrence of DNSs, in the present lower-mass ( $M_{cl}(0) \approx 3.0 \times 10^4 M_\odot$ ), primordial-binary models, is a combined consequence of (i) an overall small population of potential DNS-progenitor (primordial) binaries in such lower-mass models with a low primordial-

binary fraction ( $f_{\text{bin}} < 0.1$  for  $M_{\text{ZAMS}} < 16 M_\odot$ ; see Sec. 2), (ii) dissociation of all detached binaries, where each member would evolve into an NS, due to the associated large supernova mass loss, (iii) the stellar-wind, its tidal modification, and mass-transfer schemes adopted in the BSE (see Sec. 2.1 and references therein) that determines the pre-supernova (adiabatic) mass loss (*e.g.*, through CE ejection, regular and tidally-enhanced winds) which is instrumental in the post-supernova survival of the binary and its members' recycling, (iv) the implementation of the NSs' natal kicks in the BSE, and (v) dynamical perturbations of the potential DNS-progenitor binaries. The evolution of massive binaries in a dynamically-active environment and the consequent formation of compact binaries has not yet been well explored and is planned in a future study.

Note that even if a DNS forms through either of the channels, its members are prone to get exchanged with much more massive BHs, when the latter are ambient, limiting the lifetime of the DNS in such an environment; see below. In the present models, the only type of double-compact binaries, that is derived directly from (dynamically-processed) primordial binaries, is the NS-BH binaries (see below).

Each of the  $f_{\text{bin}} > 0$  models are found to contain several NS-BH binaries (and to rarely eject NS-BH binaries). Nearly all of such binaries are derived directly from a primordial massive binary (Sec. 2), *i.e.*, both the NS and the BH are derived from progenitors that were members of the same primordial pair. Fig. 10 shows the semi-major-axes of such NS-BH binaries, from the point of their appearance, for the  $f_{\text{bin}} \approx 10\%$  models (Table 1). Here, the semi-major-axis,  $A$ , is simply the relative separation between the NS and the BH member obtained at each NBODY7 output time, representing the width of the binary. Each of these NS-BHs are formed through detached evolution of a tight primordial binary that has avoided exchange (as indicated by the serial IDs of the NS and the BH members in the outputs), *i.e.*, they are non-recycled. The formation of the (moderately-massive) BH member through direct collapse (see Secs. 1 & 2.1 and references therein) has enabled the binary to survive the supernova mass loss, as opposed to while forming a DNS (the other factors, as raised above, being common), giving the resulting BH-NS a higher chance of survival. As for the DNS (non) formation (see above), it is impossible to capture all possible scenarios of NS-BH formation in these models, given that only a handful of the potential progenitors would exist per model.

As seen in Fig. 10, the widths of the NS-BHs, whilst they remain bound to the cluster, continue to alter due to the close encounters they experience. Their widths ultimately blow up, when, typically, the NS member gets exchanged by an intruding BH and is ejected from the binary. Such an exchange encounter limits the lifetime of an NS-BH, which, in the present models, lie between  $\sim 100$  Myr and  $\sim$  Gyr (Fig. 10); in a more massive cluster with a denser but higher-velocity dispersion BH population, the lifetime is expected to be similar<sup>11</sup>. This should also apply to any DNS that happens to be present in the cluster, where the NS members

<sup>10</sup> In this work, any hard binary between two NSs or any binary containing an NS will be regarded as an NS binary, irrespective of the NSs' recycling status. Non-recycled NS binaries, such as those assembled dynamically or formed via detached evolution of massive primordial binaries, have limited possibilities to be caught through radio observations.

<sup>11</sup> The encounter rate as seen by a binary,  $\gamma \propto \rho/\sigma$  (Banerjee & Ghosh 2006), where  $\rho$  and  $\sigma$  are the ambient stellar (BH) density and velocity dispersion, respectively. Applying the virial theorem,

are likely get exchanged sequentially by the BHs, within  $\sim$  Gyr time. Likewise the DNS case, no NS-BHs, in these models, are derived through the dynamical channel except in 1-2 cases the original BH member is exchanged with an intruder BH. In the  $f_{\text{bin}} \approx 0.1$ ,  $Z = 0.05Z_{\odot}$  model, one of the NS-BH is found to undergo GR coalescence (with an exchanged BH member; see Fig. 4) after a sequence of close encounters and ultimately triple formation with an intruder BH. Such NS-BH mergers would act as both GW sources for the LIGO and short gamma ray burst (sGRB) sources.

Note that the presence of any type of compact binary, that is derived through the internal evolution of a primordial pair (or of an exchanged stellar pair), in simulations as those here, should be taken with caution as their occurrence is dependent on the adopted stellar- and binary-evolution schemes — in the present case, on the BSE and its integration into NBODY7. Nonetheless, the small population of NS-BHs, present in the  $f_{\text{bin}} > 0$  models, could be used as probes to robustly show that the NS member of an NS binary is likely to get exchanged by a BH, within  $\sim$  Gyr after the formation of the NS binary (primordially or dynamically), when a dynamically-dominant BH population is present.

In this work, only hard double-compact binaries have been probed. Despite the near inhibition of mass segregation of the NSs (and also of other stellar members; see, Alessandrini et al. 2016; Peuten et al. 2016) due to the work of the BHs, as discussed above, they would, in principle, undergo exchange encounters with the normal-stellar binaries, potentially forming progenitors of X-ray binaries. Since the BHs continue to interact with the normal stars and their binaries (see Secs. 1, 3 & 3.1), they have the potential to acquire a stellar companion as well. Both NS-star and BH-star binaries and their possible mass-accretion phase thereafter, of course, can also appear through the internal evolution of the same primordial pair (or of an exchanged stellar pair). Finally, cataclysmic variables (CV) can appear within the models via both dynamical and binary-evolution channels. Again, as in the case of double-compact binaries (see above), a dynamically-dominant population of BHs would have the potential to quench the exchange activities of the NSs and the WDs. A more thorough analysis procedure for tracking all types of compact binaries from a larger set of such simulations is underway.

### 3.3 Remark on the dynamical binary black hole merger rate: contribution from open clusters

It would be of interest to compare the contribution of BBH merger rate from lower-mass, open- or YMC-type clusters, as considered here, with that from classical GC-type clusters considered in Monte Carlo-based studies (Sec. 1). Although open clusters and YMCs, in general, produce less BBH mergers per cluster than that from the GCs, they are more numerous, enabling them to compete with the GCs.

The present work shows that, like the GCs, the open clusters generate BBH mergers spanning their entire evolutionary time (Fig. 4). For definiteness, the GC models of Morscher et al. (2015) are considered here which have been

utilized by Rodriguez et al. (2015) for their BBH merger rate calculations. From Table 1 here, it can be observed that for the  $f_{\text{bin}} = 0$  models, increasing  $M_{cl}(0)$  by a factor of  $\approx 8$  increases the average BBH merger count, per cluster, by  $\approx 15$ ; increasing  $f_{\text{bin}}$  increases the merger count by a factor of few, for a given  $M_{cl}(0)$ . A similar scaling continues for the GC models in Morscher et al. (2015, their Table 3). Assuming that clusters are formed with a power-law mass function of index  $\approx -2$  (Gieles et al. 2006a,b; Larsen 2009), it can be noted that a shift of the lower  $M_{cl}(0)$  limit, for producing BBH mergers, to  $\approx 10^4 M_{\odot}$  (Table 1) from the GC-progenitors' lower mass limit of  $2 \times 10^5 M_{\odot}$  (Morscher et al. 2015) would increase the number of potential clusters by  $\approx 20$ . Based on the above scaling, if the average BBH merger count per cluster is reduced by a factor of  $\approx 10$  for the open-cluster/YMC progenitors with  $10^4 M_{\odot} \leq M_{cl}(0) \leq 2 \times 10^5 M_{\odot}$ , then, correspondingly, the BBH merger rate from such open clusters will be  $\approx 2$  times the GC counterpart. In other words, although YMCs and open clusters produce less BBH mergers per cluster and live shorter compared to GCs, they, altogether, would add a comparable amount to the dynamical BBH merger rate.

Note that the above estimate remains valid even after considering the “delay times” of the mergers, since both the open clusters and the GCs continue to produce BBH mergers throughout their  $\gtrsim 10$  Gyr lifespan (*c.f.* Fig. 4 here and Fig. 1 of Chatterjee et al. 2017b). In other words, the comparison remains valid even when the BBH mergers occurring at the current epoch (within redshift  $z \lesssim 0.2$ ) are considered. Such a semi-quantitative comparison, of course, depends on the mass threshold of what can be called a progenitor of a GC (here taken to be  $M_{cl}(0) \approx 2 \times 10^5 M_{\odot}$  for specificity). A more proper derivation of the BBH merger rate, including the open-type clusters, can be done by combining the BBH mergers from lower-mass direct N-body models as here with those from the massive Monte Carlo models, and following the cosmic star (cluster) formation and metallicity evolution as done in, *e.g.*, Bulik et al. (2004); Belczynski et al. (2016). Such a study is planned in the near future with a more elaborate set of direct N-body models.

## 4 SUMMARY

The study of the dynamics of stellar-remnant BHs in YMCs and open clusters, that has been initiated in Paper I, is extended in this study to include more massive clusters ( $M_{cl}(0) \lesssim 10^5 M_{\odot}$ ) and primordial binaries (Sec. 2; Table 1). The key inferences are as follows:

- For all clusters with initial masses up to  $M_{cl}(0) \lesssim 10^5 M_{\odot}$  at least and with compact sizes (here taken to be  $r_h(0) \approx 2$  pc), the GR BBH mergers mostly take place in situ, within triples that are bound to the cluster (Table 1, Fig. 4). The apparent contrast with the outcomes of Monte Carlo calculations of  $\sim 10$  times more massive clusters, which predominantly yield mergers in BBHs that are dynamically ejected from them, is a consequence of the lower-mass open clusters having lower escape speeds and hence containing and ejecting generally wider BBHs (Sec. 3.1). However, a difference would also arise due to the more elaborate and complete treatments of close encounters and of relativistic, few-body sub-systems, in direct N-body approaches as here (Sec. 2.1

since both  $\rho$  and  $\sigma \propto M$ , the (BH) cluster mass,  $\gamma$  is independent of  $M$  and depends only on the cluster's scale length.

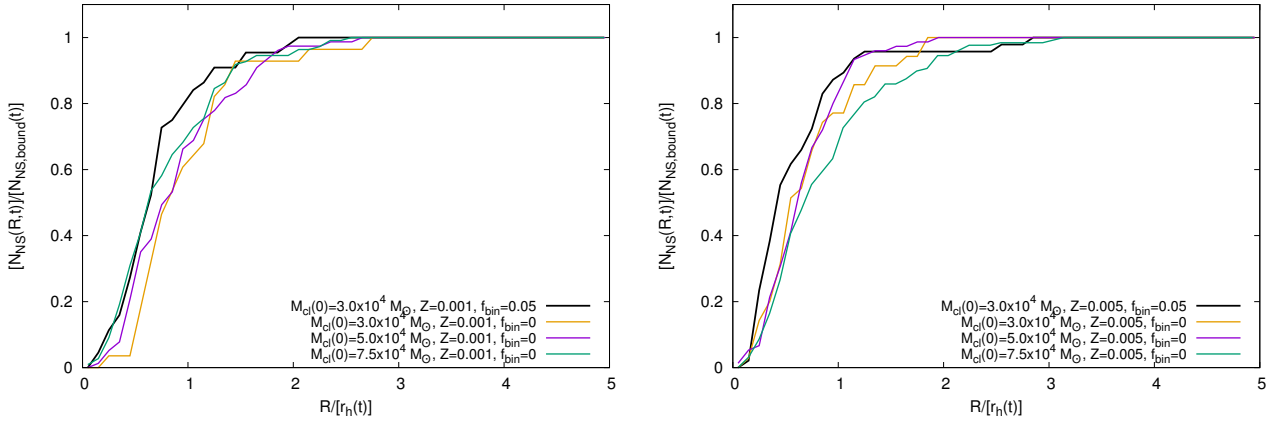


**Figure 9.** The normalized cumulative radial distribution of NSs, as in Fig. 8, at  $\approx 10$  Gyr evolutionary time and for the models with  $3.0 \times 10^4 M_\odot \lesssim M_{cl}(0) \lesssim 7.5 \times 10^4 M_\odot$  (legends) and  $Z = 0.05Z_\odot$  (left panel) and  $0.25Z_\odot$  (right panel). Those for the computed models with  $f_{bin} \approx 5\%$  overall binary fraction (Table 1) are shown in the black lines. A higher rate of BH depletion, in the presence of primordial binaries (Fig. 3; Sec. 3), aids the mass segregation of the NSs, making them somewhat more centrally concentrated at 10 Gyr, compared to the cases with no primordial binaries.

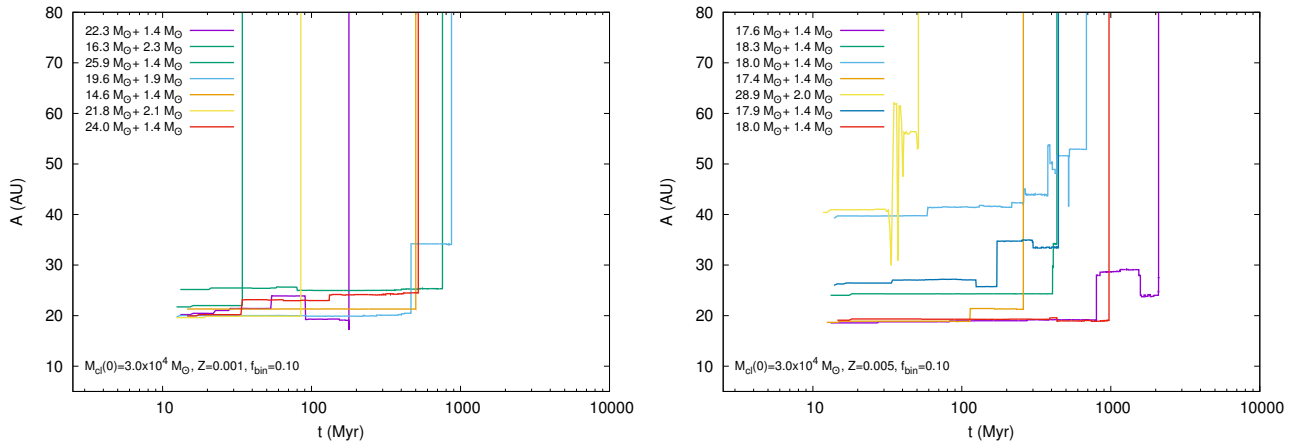


**Figure 10.** The time evolution of the semi-major-axes,  $A$ , of the NS-BH binaries present in the computed models with  $M_{cl}(0) \approx 3.0 \times 10^4 M_\odot$  and  $f_{bin} \approx 10\%$  (Table 1). Each line follows a particular NS-BH binary, with member masses as indicated in the legends. All NS-BH binaries, that appear in these models (as well as in the other ones with primordial binaries; see Table 1), are formed through the evolution of (possibly dynamically-modified) primordial binaries. Their lifetimes, in the clusters, vary from  $\sim 100$  Myr to  $\sim$  Gyr, by which time the pairs get destroyed, often through exchange interactions (Sec. 3.2). Typically, such binaries are born several 10s of AUs wide and they retain sizes of that order until their destructions (true for the NS-BH binaries in the other primordial-binary models also).

and references therein). In any case, the BBH merger counts per cluster and the delay times of the mergers, as obtained here for the open clusters, follow qualitatively similar trends with cluster mass, primordial-binary content, and BBH parameters as those in the Monte Carlo GC models (Sec. 3.3 and references therein). Based on such trends, it can be qualitatively inferred that open clusters would contribute to the present-epoch (low-redshift) dynamical BBH merger rate to a similar extent as the GCs.

- The introduction of a small population of primordial binaries ( $f_{bin} \gtrsim 0.05$  overall binary fraction, with  $f_{Obin} \approx 1.0$  for the O-stars; Sec. 2) in the model clusters tends to increase the number of in situ BBH coalescences significantly (Table 1). However, in all the  $f_{bin} > 0$  computations here, all the in situ (and also the few ejected) BBH mergers involve BHs that were members of different primordial pairs, *i.e.*,

the coalescing binaries have been assembled, through exchange interactions, with independently-born BHs. Hence, if these BHs have finite spins, all of these mergers will be spin-orbit misaligned as indicated in the GW170104 event (Sec. 1 and references therein). Besides spin-orbit misalignment, the BBH-merger mass ratio being substantially less than unity, especially being  $M_{BH2}/M_{BH1} \lesssim 0.7$ , would serve as an additional indication of a dynamical assembly of the BBH (Sec. 3.1, Fig. 6).

- Among all the to-date confirmed LIGO GW events (*i.e.*, excluding LVT151012), the limits of GW170104's parameters encompass the highest fraction of the BBH mergers obtained here (Fig. 4, Sec. 3.1). All the coalescing BBHs, obtained here, have high eccentricities (owing to resonant triples/Kozai mechanism or strong dynamical perturbation while getting ejected) when they have been emitting GW in



the LISA band or in sub-LISA frequencies. They circularize sufficiently while traversing the LISA band so that they become potentially audible by the LISA ( $e \lesssim 0.7$ ) and are nearly circularized in when they reach the LIGO band (Sec. 3.1.1; Fig. 7). The most eccentric BBHs in the LIGO band, here, have  $10^{-2} < e < 10^{-1}$ .

- The energy injection by the BHs into the host cluster (Secs. 1,3; see also Paper I) inhibits the regular two-body interaction—driven mass segregation of less-massive entities; in particular, of the NSs (Figs. 8 & 9). This prevents the NSs to effectively participate in exchange interactions as long as a dynamically-dominant BH population is present. Especially, like with the NS-BH binaries (non-recycled; see Sec. 3.2) present in the model clusters here, the NS member(s) in any NS binary would get exchanged with an intruder BH in  $\lesssim 1$  Gyr time (Fig. 10, Sec. 3.2).

## ACKNOWLEDGEMENTS

SB is thankful to the anonymous referee for helpful comments that has improved some of the descriptions in this paper. SB is indebted to Sverre Aarseth of the Institute of Astronomy, Cambridge, for his efforts in improving NBODY6/7, without which this study would not have been possible. SB is thankful to Sverre Aarseth also for reading the manuscript and providing improvement suggestions. SB is thankful to the computing team of the Argelander-Institut für Astronomie, University of Bonn, for their efficient maintenance of the workstations on which all the computations have been performed.

Table 1: Summary of model evolutionary calculations. The columns from left to right respectively denote: (a) initial mass,  $M_{cl}(0)$ , of the model cluster, (b) initial half-mass radius,  $r_h(0)$ , (c) metallicity,  $Z$ , (d) overall primordial binary fraction,  $f_{bin}$  (see Sec. 2), (e) total evolutionary time,  $T_{evol}$ , of the model, (f) the number of (triple-mediated) binary black hole (BBH) coalescences,  $N_{mrg,in}$ , that occurred within the clusters, (g) the number of BBH coalescences (in BBHs that are ejected from the clusters),  $N_{mrg,out}$ , that occurred outside the clusters within the Hubble time. The coalescing masses (in  $M_\odot$ ), and the evolutionary times,  $t_{mrg}(t_{ej})$ , of the occurrences of the individual coalescences (ejections; in Myr) are given in columns (f) & (g). This table includes the new N-body computations (Sec. 2) and as well those from Banerjee (2017, Paper I).

$M_{cl}(0)/M_\odot$	$r_h(0)/pc$	$Z/Z_\odot$	$f_{bin}$	$T_{evol}/Gyr$	$N_{mrg,in}$	$N_{mrg,out}$
$1.0 \times 10^5$	2.0	0.05	0.0	1	3 (57.7+28.0; 120.0), (53.1+32.9; 165.1), (40.3+55.4; 286.3)	0
$1.0 \times 10^5$	2.0	0.25	0.0	1	4 (37.9+40.5; 102.9), (20.3+37.1; 179.3), (18.2+32.0; 188.6), (29.1+34.8; 246.6)	0
$1.0 \times 10^5$	2.0	0.50	0.0	1	0	1 (24.8+19.0; 625.3)
$7.5 \times 10^4$	2.0	0.05	0.0	10	7 (40.4+64.2; 56.8), (43.0+44.3; 200.4), (24.8+28.6; 543.9), (31.1+22.8; 909.2), (21.3+25.9; 1852.5), (24.4+26.0; 4417.1), (10.6+22.4; 10010.6)	0
$7.5 \times 10^4$	2.0	0.25	0.0	10	2 (37.8+32.8; 76.5), (17.5+10.1; 10298.6)	1 (22.8+27.6; 508.3)
$^1 5.0 \times 10^4$	2.0	0.05	0.0	> 10	1 (24.3+17.7; 2466.1)	1 (26.0+42.8; 603.0)
$^1 5.0 \times 10^4$	2.0	0.25	0.0	> 10	1 (34.5+22.7; 151.5)	0
$^1 5.0 \times 10^4$	2.0	1.00	0.0	10	3 (9.0+7.5; 5210.1), (10.6+9.4; 7171.0), (9.1+9.0; 8117.7)	0
$^1 3.0 \times 10^4$	2.0	0.05	0.0	> 10	1 (38.1+25.9; 933.8)	2 (25.7+13.8; 1828.0), (23.6+22.3; 4464.1)
$^1 3.0 \times 10^4$	2.0	0.25	0.0	> 10	0	2 (35.3+20.3; 1787.1), (15.7+12.2; 12463.7)
$^1 3.0 \times 10^4$	2.0	1.00	0.0	> 10	1 (10.6+9.0; 3495.9)	0
$^1 1.5 \times 10^4$	2.0	0.05	0.0	> 10	1 (49.4+30.9; 109.7)	0
$^1 1.5 \times 10^4$	1.0	0.25	0.0	5	0	0
$^1 1.0 \times 10^4$	2.0	0.05	0.0	9	0	0
$^1 1.0 \times 10^4$	1.0	0.05	0.0	5	1 (43.6+34.5; 153.8)	0
$^1 1.0 \times 10^4$	1.0	0.25	0.0	5	0	0
$^1 0.7 \times 10^4$	1.0	0.05	0.0	7	0	0
$3.0 \times 10^4$	2.0	0.05	0.02	10	0	1 (25.9+27.2; 1410.9)
$3.0 \times 10^4$	2.0	0.25	0.02	10	2 (19.0+17.2; 3513.1), (18.9+16.2; 5185.2)	0
$3.0 \times 10^4$	2.0	0.05	0.05	10	1 (22.4+14.8; 6838.7)	0
$3.0 \times 10^4$	2.0	0.25	0.05	10	4 (33.3+34.8; 490.3), (34.5+33.8; 799.8), (17.5+22.6; 3368.0), (17.2+13.5; 6649.7)	0
$3.0 \times 10^4$	2.0	0.05	0.1	10	3 (37.9+36.3; 340.2), (28.0+1.85; 1561.0),	0

Continued on next page

**Table 1 – continued from previous page**

$M_{cl}(0)/M_{\odot}$	$r_h(0)/\text{pc}$	$Z/Z_{\odot}$	$f_{\text{bin}}$	$T_{\text{evol}}/\text{Gyr}$	$N_{\text{mrg},\text{in}}$	$N_{\text{mrg},\text{out}}$
					(21.3+13.3; 10025.2)	
$3.0 \times 10^4$	2.0	0.25	0.1	6	3 (38.8+12.3; 307.0), (18.2+21.2; 383.2), (17.7+17.6; 5310.3)	0

<sup>1</sup> From [Banerjee \(2017\)](#).

## References

- Aarseth S. J., 2003, Gravitational N-Body Simulations
- Aarseth S. J., 2012, *MNRAS*, **422**, 841
- Abbott B. P., et al., 2016a, *Phys. Rev. X*, **6**, 041014
- Abbott B. P., et al., 2016b, *Phys. Rev. X*, **6**, 041015
- Abbott B. P., et al., 2016c, *Physical Review Letters*, **116**, 061102
- Abbott B. P., et al., 2016d, *Physical Review Letters*, **116**, 241103
- Abbott B. P., et al., 2016e, *ApJ*, **818**, L22
- Abbott B. P., et al., 2017, *Physical Review Letters*, **118**, 221101
- Alessandrini E., Lanzoni B., Ferraro F. R., Miocchi P., Vesperini E., 2016, *ApJ*, **833**, 252
- Amaro-Seoane P., et al., 2017, ArXiv e-prints (arXiv:1702.00786),
- Antonini F., Rasio F. A., 2016, *ApJ*, **831**, 187
- Antonini F., Murray N., Mikkola S., 2014, *ApJ*, **781**, 45
- Antonini F., Chatterjee S., Rodriguez C. L., Morscher M., Pattabiraman B., Kalogera V., Rasio F. A., 2016, *ApJ*, **816**, 65
- Antonini F., Toonen S., Hamers A. S., 2017, *ApJ*, **841**, 77
- Arca-Sedda M., 2016, *MNRAS*, **455**, 35
- Askar A., Szkudlarek M., Gondek-Rosińska D., Giersz M., Bulik T., 2016, *Monthly Notices of the Royal Astronomical Society: Letters*, **464**, L36
- Banerjee S., 2017, *MNRAS*, **467**, 524
- Banerjee S., Ghosh P., 2006, *MNRAS*, **373**, 1188
- Banerjee S., Kroupa P., 2011, *ApJ*, **741**, L12
- Banerjee S., Baumgardt H., Kroupa P., 2010, *MNRAS*, **402**, 371
- Baumgardt H., 2017, *MNRAS*, **464**, 2174
- Belczynski K., Kalogera V., Bulik T., 2002, *The Astrophysical Journal*, **572**, 407
- Belczynski K., Kalogera V., Rasio F. A., Taam R. E., Zezas A., Bulik T., Maccarone T. J., Ivanova N., 2008, *The Astrophysical Journal Supplement Series*, **174**, 223
- Belczynski K., Lorimer D. R., Ridley J. P., Curran S. J., 2010a, *MNRAS*, **407**, 1245
- Belczynski K., Bulik T., Fryer C. L., Ruiter A., Valsecchi F., Vink J. S., Hurley J. R., 2010b, *The Astrophysical Journal*, **714**, 1217
- Belczynski K., Holz D. E., Bulik T., O'Shaughnessy R., 2016, *Nature*, **534**, 512
- Belczynski K., et al., 2017, preprint, (arXiv:1706.07053)
- Bovill M. S., Puzia T. H., Ricotti M., Taylor M. A., 2016, *ApJ*, **832**, 88
- Brassington N. J., et al., 2010, *ApJ*, **725**, 1805
- Breen P. G., Heggie D. C., 2013a, *Monthly Notices of the Royal Astronomical Society*, **432**, 2779
- Breen P. G., Heggie D. C., 2013b, *Monthly Notices of the Royal Astronomical Society*, **436**, 584
- Brem P., Amaro-Seoane P., Spurzem R., 2013, *MNRAS*, **434**, 2999
- Bulik T., Belczyński K., Rudak B., 2004, *A&A*, **415**, 407
- Campanelli M., Lousto C., Zlochower Y., Merritt D., 2007, *ApJ*, **659**, L5
- Chatterjee S., Rodriguez C. L., Rasio F. A., 2017a, *ApJ*, **834**, 68
- Chatterjee S., Rodriguez C. L., Kalogera V., Rasio F. A., 2017b, *ApJ*, **836**, L26
- Chen X., Amaro-Seoane P., 2017, *ApJ*, **842**, L2
- De Mink S. E., Mandel I., 2016, *MNRAS*, **460**, 3545
- De Mink S. E., Cantiello M., Langer N., Pols O. R., Brott I., Yoon S.-C., 2009, *A&A*, **497**, 243
- Downing J. M. B., Benacquista M. J., Giersz M., Spurzem R., 2010, *Monthly Notices of the Royal Astronomical Society*, **407**, 1946
- Downing J. M. B., Benacquista M. J., Giersz M., Spurzem R., 2011, *MNRAS*, **416**, 133
- Duquennoy A., Mayor M., 1991, *A&A*, **248**, 485
- Farr W. M., Stevenson S., Miller M. C., Mandel I., Farr B., Vecchio A., 2017, preprint, (arXiv:1706.01385)
- Gieles M., Larsen S. S., Scheepmaker R. A., Bastian N., Haas M. R., Lamers H. J. G. L. M., 2006a, *A&A*, **446**, L9
- Gieles M., Larsen S. S., Bastian N., Stein I. T., 2006b, *A&A*, **450**, 129
- Giersz M., Heggie D. C., Hurley J. R., Hypki A., 2013, *MNRAS*, **431**, 2184
- Harris W. E., 1996, *AJ*, **112**, 1487
- Heggie D. C., 1975, *MNRAS*, **173**, 729
- Heggie D., Hut P., 2003, The Gravitational Million-Body Problem: A Multidisciplinary Approach to Star Cluster Dynamics
- Heiter U., Soubiran C., Netopil M., Paunzen E., 2014, *A&A*, **561**, A93
- Hénon M., 1975, in Hayli A., ed., IAU Symposium Vol. 69, Dynamics of the Solar Systems. p. 133
- Hoang B.-M., Naoz S., Kocsis B., Rasio F. A., Dosopoulou F., 2017, preprint, (arXiv:1706.09896)
- Huerta E. A., Brown D. A., 2013, *Phys. Rev. D*, **87**, 127501
- Hughes S. A., 2009, *ARA&A*, **47**, 107
- Hurley J. R., Pols O. R., Tout C. A., 2000, *Monthly Notices of the Royal Astronomical Society*, **315**, 543
- Hurley J. R., Tout C. A., Pols O. R., 2002, *Monthly Notices of the Royal Astronomical Society*, **329**, 897
- Hurley J. R., Sippel A. C., Tout C. A., Aarseth S. J., 2016, *Publ. Astron. Soc. Australia*, **33**, e036
- Hut P., Bahcall J. N., 1983, *ApJ*, **268**, 319
- Hut P., Verbunt F., 1983, *Nature*, **301**, 587
- Kimpson T. O., Spera M., Mapelli M., Ziosi B. M., 2016, *MNRAS*, **463**, 2443
- Kozai Y., 1962, *The Astronomical Journal*, **67**, 591
- Kroupa P., 1995a, *MNRAS*, **277**, 1491
- Kroupa P., 1995b, *MNRAS*, **277**, 1507
- Kroupa P., 2001, *MNRAS*, **322**, 231
- Kroupa P., Weidner C., Pflamm-Altenburg J., Thies I., Dabringhausen J., Marks M., Maschberger T., 2013, The Stellar and Sub-Stellar Initial Mass Function of Simple and Composite Populations. p. 115, doi:10.1007/978-94-007-5612-0\_4
- Kulkarni S. R., Hut P., McMillan S., 1993, *Nature*, **364**, 421
- Larsen S. S., 2009, *Astronomy and Astrophysics*, **494**, 539
- Lithwick Y., Naoz S., 2011, *ApJ*, **742**, 94
- Lorimer D. R., 2008, *Living Reviews in Relativity*, **11**
- Lützgendorf N., et al., 2016, in Meiron Y., Li S., Liu F.-K., Spurzem R., eds, IAU Symposium Vol. 312, Star Clusters and Black Holes in Galaxies across Cosmic Time. pp 181–188 (arXiv:1501.07441), doi:10.1017/S1743921315007784
- Maccarone T. J., Kundu A., Zepf S. E., Rhode K. L., 2007, *Nature*, **445**, 183
- Mackey A. D., Wilkinson M. I., Davies M. B., Gilmore G. F., 2007, *MNRAS*, **379**, L40
- Mackey A. D., Wilkinson M. I., Davies M. B., Gilmore G. F., 2008, *MNRAS*, **386**, 65
- Mapelli M., 2016, *MNRAS*, **459**, 3432
- Marchant P., Langer N., Podsiadlowski P., Tauris T. M., Moriya T. J., 2016, *A&A*, **588**, A50
- Marks M., Kroupa P., Oh S., 2011, *MNRAS*, **417**, 1684
- Mikkola S., Aarseth S. J., 1993, *Celestial Mechanics & Dynamical Astronomy*, **57**, 439
- Mikkola S., Aarseth S., 2002, *Celestial Mechanics and Dynamical Astronomy*, **84**, 343
- Mikkola S., Merritt D., 2008, *The Astronomical Journal*, **135**, 2398
- Mikkola S., Tanikawa K., 1999, *Monthly Notices of the Royal Astronomical Society*, **310**, 745
- Miller M. C., Hamilton D. P., 2002, *ApJ*, **576**, 894
- Miller-Jones J. C. A., et al., 2015, *MNRAS*, **453**, 3918
- Morscher M., Umbreit S., Farr W. M., Rasio F. A., 2013, *ApJ*, **763**, L15
- Morscher M., Pattabiraman B., Rodriguez C., Rasio F. A., Umbreit S., 2015, *The Astrophysical Journal*, **800**, 9
- Nishizawa A., Berti E., Klein A., Sesana A., 2016, *Phys. Rev. D*, **94**, 064020



- Nishizawa A., Sesana A., Berti E., Klein A., 2017, *MNRAS*, **465**, 4375
- Nitadori K., Aarseth S. J., 2012, *Monthly Notices of the Royal Astronomical Society*, **424**, 545
- O’Shaughnessy R., Gerosa D., Wysocki D., 2017a, *Physical Review Letters*, **119**, 011101
- O’Shaughnessy R., Bellovary J. M., Brooks A., Shen S., Governato F., Christensen C. R., 2017b, *MNRAS*, **464**, 2831
- Oh S., Kroupa P., Pflamm-Altenburg J., 2015, *ApJ*, **805**, 92
- Ośłowski S., Bulik T., Gondek-Rosińska D., Belczyński K., 2011, *MNRAS*, **413**, 461
- Park D., Kim C., Lee H. M., Bae Y.-B., Belczynski K., 2017, *MNRAS*, **469**, 4665
- Peters P. C., 1964, *Physical Review*, **136**, 1224
- Peuten M., Zocchi A., Gieles M., Gualandris A., Hénault-Brunet V., 2016, *MNRAS*, **462**, 2333
- Podsiadlowski P., Langer N., Poelarends A. J. T., Rappaport S., Heger A., Pfahl E., 2004, *The Astrophysical Journal*, **612**, 1044
- Portegies Zwart S. F., McMillan S. L. W., 2000, *ApJ*, **528**, L17
- Portegies Zwart S. F., McMillan S. L. W., Gieles M., 2010, *ARA&A*, **48**, 431
- Ransom S. M., 2008a, in Vesperini E., Giersz M., Sills A., eds, IAU Symposium Vol. 246, Dynamical Evolution of Dense Stellar Systems. pp 291–300, [doi:10.1017/S1743921308015810](https://doi.org/10.1017/S1743921308015810)
- Ransom S. M., 2008b, in Bassa C., Wang Z., Cumming A., Kaspi V. M., eds, American Institute of Physics Conference Series Vol. 983, 40 Years of Pulsars: Millisecond Pulsars, Magnetars and More. pp 415–423 ([arXiv:0710.3626](https://arxiv.org/abs/0710.3626)), [doi:10.1063/1.2900267](https://doi.org/10.1063/1.2900267)
- Rantala A., Pihajoki P., Johansson P. H., Naab T., Lahén N., Sawala T., 2017, *ApJ*, **840**, 53
- Rodriguez C. L., Morscher M., Pattabiraman B., Chatterjee S., Haster C.-J., Rasio F. A., 2015, *Phys. Rev. Lett.*, **115**
- Rodriguez C. L., Chatterjee S., Rasio F. A., 2016a, *Physical Review D*, **93**
- Rodriguez C. L., Morscher M., Wang L., Chatterjee S., Rasio F. A., Spurzem R., 2016b, *MNRAS*, **463**, 2109
- Rodriguez C. L., Haster C.-J., Chatterjee S., Kalogera V., Rasio F. A., 2016c, *ApJ*, **824**, L8
- Samsing J., Ramirez-Ruiz E., 2017, *ApJ*, **840**, L14
- Samsing J., MacLeod M., Ramirez-Ruiz E., 2014, *ApJ*, **784**, 71
- Sana H., Evans C. J., 2011, in Neiner C., Wade G., Meynet G., Peters G., eds, IAU Symposium Vol. 272, Active OB Stars: Structure, Evolution, Mass Loss, and Critical Limits. pp 474–485 ([arXiv:1009.4197](https://arxiv.org/abs/1009.4197)), [doi:10.1017/S1743921311011124](https://doi.org/10.1017/S1743921311011124)
- Sana H., et al., 2013, *A&A*, **550**, A107
- Sesana A., 2016, *Physical Review Letters*, **116**, 231102
- Sigurdsson S., Hernquist L., 1993, *Nature*, **364**, 423
- Silber K., Tremaine S., 2017, *ApJ*, **836**, 39
- Sippel A. C., Hurley J. R., 2013, *MNRAS*, **430**, L30
- Sollima A., et al., 2016, *MNRAS*, **462**, 1937
- Spera M., Mapelli M., Bressan A., 2015, *Mon. Not. R. Astron. Soc.*, **451**, 4086
- Spitzer L., 1987, Dynamical evolution of globular clusters
- Strader J., Chomiuk L., Maccarone T. J., Miller-Jones J. C. A., Seth A. C., 2012, *Nature*, **490**, 71
- Tauris T. M., et al., 2017, preprint, ([arXiv:1706.09438](https://arxiv.org/abs/1706.09438))
- Taylor M. A., Puzia T. H., Gomez M., Woodley K. A., 2015, *ApJ*, **805**, 65
- Wang L., Spurzem R., Aarseth S., Nitadori K., Berczik P., Kouwenhoven M. B. N., Naab T., 2015, *Monthly Notices of the Royal Astronomical Society*, **450**, 4070
- Wang L., et al., 2016, *Mon. Not. R. Astron. Soc.*, **458**, 1450
- Weidner C., Kroupa P., 2004, *MNRAS*, **348**, 187
- Wen L., 2003, *ApJ*, **598**, 419
- Ziosi B. M., Mapelli M., Branchesi M., Tormen G., 2014, *MNRAS*, **441**, 3703